

Chemical composition of tourmaline in orogenic gold deposits

Marjorie Sciuba^{1,2}, Georges Beaudoin^{1,2}, Sheida Makvandi^{1,2}

✉ Marjorie Sciuba

Marjorie.sciuba@gmail.com

✉ Georges Beaudoin

Georges.Beaudoin@ggl.ulaval.ca

¹ Département de Géologie et Génie Géologique, Université Laval, Québec (QC) G1V 0A6, Canada

² Centre de recherche sur la géologie et l'ingénierie des ressources minérales (E4m), Université Laval, Québec (QC) G1V 0A6, Canada

Abstract

Tourmaline from eighteen orogenic gold deposits and districts, hosted in varied country rocks and metamorphic facies, was investigated by EPMA (Electron Probe Micro-Analyzer) and LA-ICP-MS (Laser Ablation-Inductively Coupled Plasma-Mass Spectrometry) to establish discriminant geochemical features to constrain indicator mineral surveys for gold exploration. Such tourmaline most commonly belongs to the alkali group, with a dravitic composition. LA-ICP-MS results were investigated with binary plots and PLS-DA (Partial Least Square-Discriminant Analysis). PLS-DA suggests that the major element composition of tourmaline from orogenic gold deposits is buffered by the hydrothermal fluid, whereas trace element composition is strongly controlled by the composition and the metamorphic facies of the country rocks. Contents of Sn, Ga, Ti, Rare Earth Elements (REE), Zr, Hf, Nb, Ta, Th and U vary with the metamorphic facies of the country rocks. Tourmaline from orogenic gold deposits has high contents of Sr, V, and Ni and low Li, Be, Ga, Sn, Nb, Ta, U, and Th compared to tourmaline from other deposit types and geological environments. Binary plots such as Sr/Li vs. V/Sn, Sr/Sn vs. V/Nb, Sr/Sn vs. Ni/Nb and Sr/Sn vs. V/Be, as well as PLS-DA, discriminate tourmaline from orogenic gold deposits from that of other settings. Binary plots highlight a transitional variation in the trace element composition of tourmaline from metamorphic, to magmatic-hydrothermal, to magmatic environments.

Keywords: tourmaline, orogenic gold, trace elements, partial least square-discriminant analysis

25 **Introduction**

26 Tourmaline is commonly associated with mineralization in orogenic gold deposits where it is a major to accessory
27 mineral in veins and in proximal to intermediate-scale alteration zones in sub-greenschist to amphibolite facies
28 settings (Goldfarb et al. 2005; Eilu et al. 1999). Tourmaline formation in orogenic gold deposits (e.g. Val-d'Or, Canada;
29 Mount Gibson and Big Bell, Western Australia) is contemporaneous with gold mineralization (Anglin et al. 1996;
30 Garofalo et al. 2002; Jiang et al. 2002; Beaudoin and Pitre 2005). In several deposits, tourmaline may precede, or less
31 commonly postdate, gold precipitation but is part of the gold-bearing veins (Goldfarb et al. 2005).

32 Tourmaline forms in a wide range of pressure-temperature conditions (up to 6-8 GPa, Krosse 1995; up to 800-850°C,
33 Ota et al. 2008) and, occurs in a broad range of geological settings including metamorphic, magmatic, and
34 hydrothermal (Henry and Dutrow 1996; Dutrow and Henry 2011; Van Hinsberg et al. 2011). Magmatic tourmaline
35 includes occurrences in pegmatites, and granites whereas hydrothermal tourmaline is found in greisen, porphyry
36 Cu±Mo, Cu–Au breccia pipes, Sn–W veins, iron oxide-copper-gold (IOCG), shear zone-hosted U-Cu, sedimentary-
37 exhalative (SEDEX), volcanogenic massive sulfide (VMS) and unconformity-associated U, in addition to orogenic gold
38 deposits (Slack 1996; Slack and Trumbull 2011). Metamorphic tourmaline is found in diverse settings in
39 metamorphosed rocks (Galbraith et al. 2009; Marks et al. 2013; Wang et al. 2018).

40 Tourmaline is a complex borosilicate ($XY_3Z_6[T_6O_{18}](BO_3)_3V_3W$) with three major end-members reflecting the major
41 element present in the Y site: Fe-rich schorl, Mg-rich dravite and Li-rich elbaite (Henry et al. 2011). A wide range of
42 elements is able to substitute in the tourmaline structure as major, minor or trace elements including Na, Ca, K, Mn, Al,
43 Cr, Si, Be, Ti, Zn, Cr, Ni, Cu, Sn, Ga, Sc, V, Ga, Sc, Rb, Cs, Sr, Y, REE, Pb, Ag, F, Cl and Br (Dietrich 1985; Henry et al. 2011;
44 Marschall and Jiang 2011). Several studies document the major and minor element composition, but only a few report
45 trace element compositions of tourmaline from orogenic gold deposits (Jiang et al. 2002; Deksissa and Koeberl 2004;
46 Hazarika et al. 2015; Hazarika et al. 2016; Grzela 2017; Manégliá 2017; Kalliomäki et al. 2017). The trace element
47 composition of tourmaline from various environments and deposit types are also available, including porphyry Cu-Mo
48 (Koval et al. 1991; Yavuz et al. 1999; Iveson et al. 2016), VMS (Hellingwerf et al. 1994; Griffin et al. 1996; Slack et al.
49 1999), Sn skarn (Jiang et al. 2004), SEDEX (Griffin et al. 1996; Klemme et al. 2011), W-Sn (Harlaux 2016; Duchoslav et
50 al. 2017; Hong et al. 2017); Sn (Harlaux et al. 2018; Harlaux et al. 2019); polymetallic Pb-Zn-Cu±U (Yavuz et al. 2011);
51 polymetallic Sn-Ag-Pb-Zn (Jiang et al. 1999); U unconformity-related (Joyce 2016) deposits, pegmatites (Jolliff et al.
52 1987; Roda et al. 1995; Roda-Robles et al. 2004; Roda-Robles et al. 2011; Bačik et al. 2012; Gadas et al. 2012; Roda-

53 Robles et al. 2012; Čopjaková et al. 2013; Marks et al. 2013; Roda-Robles et al. 2015; Hazarika et al. 2017), and granites
54 (Drivenes et al. 2015; Yang et al. 2015b; Hong et al. 2017; Kalliomäki et al. 2017; Tahmasbi et al. 2017).

55 Previous studies showed that the major element composition of tourmaline records bulk rock and fluid compositions
56 in metasomatic and metamorphic environments (Taylor and Slack 1984; Lottermoser and Plimer 1987; Slack and Coad
57 1989; Gallagher and Kennan 1992). For example, high Li concentration is typical of magmatic tourmaline in pegmatites
58 and granites (Keller et al. 1999; Selway et al. 1999; Selway et al. 2000; Drivenes et al. 2015; Kalliomäki et al. 2017),
59 whereas high Sn is common in Sn deposits (Jiang et al. 1999; Williamson et al. 2000; Duchoslav et al. 2017; Hong et al.
60 2017; Harlaux et al. 2018). Drivenes et al. (2015) proposed that Sn concentration is a good indicator for Sn magmatic
61 fertility, such that the Sn concentration is high in tourmaline associated with Sn mineralization and low in barren
62 granites. Hong et al. (2017) used high Sn and Zn/Nb, Co/Nb, Sr/Ta, and Co/La ratios to discriminate tourmaline host
63 rock composition of fertile from barren Sn granites. In alteration zones with low fluid/rock ratios, such as the Broken
64 Hill deposit, protolith composition exerts a strong control on tourmaline major element signature (Slack et al. 1993),
65 whereas deposits formed at high fluid/rock ratios, such as VMS deposit feeder zones, tourmaline major element
66 composition is buffered by the fluid (Slack and Coad 1989; Slack and Trumbull 2011). Other workers have shown that
67 tourmaline composition in magmatic to hydrothermal environments depends on pressure, temperature, salinity of the
68 hydrothermal fluid and host rock composition (Henry and Dutrow 1996; Van Hinsberg and Schumacher 2007; Ertl et
69 al. 2008; Van Hinsberg and Schumacher 2009; Slack and Trumbull 2011; Orlando et al. 2017). For example, schorl is
70 more common in magmatic rocks whereas dravite is typical of SEDEX and VMS hydrothermal assemblages (Slack
71 1996). Povondraite tourmaline forms preferentially from highly saline fluids (Henry et al. 2008; Van Hinsberg and
72 Schumacher 2011). Trace element compositions also reflect the bulk composition of the host rocks (Raith et al. 2004;
73 Van Hinsberg and Schumacher 2011; Yang et al. 2015a; Kalliomäki et al. 2017) and may be indicative of the fluid origin
74 (Griffin et al. 1996). Copper, Pb and Zn in tourmaline from VMS and SEDEX deposits reflect the major commodities in
75 the associated mineralization (Griffin et al. 1996). Baksheev et al. (2012) suggested that tourmaline has a good
76 potential to distinguish the type of porphyry deposit (Cu, Au and Sn) based on variation in Mg, F, and Fe_{tot} contents,
77 and Fe^{3+}/Fe_{tot} ratio. Duchoslav et al. (2017) reported that, in the Cornubian Batholith (England), hydrothermal
78 tourmaline is Sn-rich and Ti-, Cr- and V-poor compared to late-magmatic tourmaline.

79 The physical and chemical properties of tourmaline are ideal for use as an indicator mineral for exploration for
80 orogenic gold deposits. Tourmaline is resistant to weathering and can survive long-distance transport. With a specific
81 gravity ranging from 2.9 to 3.1 g/cm³, tourmaline can be separated by density in heavy mineral concentrates. However,

82 the origin of tourmaline found in heavy mineral concentrates cannot yet be constrained. Here, we study tourmaline
83 composition from gold-bearing veins from orogenic gold deposits, and from other geological settings. We test the
84 influence of country rock composition, local metamorphic facies and age of the deposit on the tourmaline composition.
85 Our results are compared with data from literature in order to identify trace elements that may discriminate
86 tourmaline from gold-bearing veins from orogenic gold deposits from that derived from other deposit types and
87 geological environments, and to establish criteria for indicator mineral surveys to constrain the source of tourmaline
88 and thus guide mineral exploration.

89 **Geological setting of selected orogenic gold deposits**

90 Tourmaline was investigated from gold-bearing veins from 18 orogenic gold deposits and districts (Table 1) including
91 eight world-class deposits as defined by Goldfarb et al. (2005). The selected deposits present diverse geological
92 settings with different bulk country rock compositions, metamorphic facies and age of country rocks, as well as age
93 and style of mineralization, and cover the range of major features described for orogenic gold deposits (Table 1).
94 Country rocks of the selected deposits vary from clastic sedimentary, and volcanic (tholeiitic basalt, komatiite), to
95 plutonic (syenite, granite, gabbro). Country rocks are metamorphosed from lower greenschist (e.g. Essakane) to the
96 upper amphibolite facies (e.g. New Consort). Archean ages are most common for tourmaline-bearing orogenic gold
97 deposits. At Essakane and Navachab, country rocks are Proterozoic, whereas at Excelsior and Salsigne, country rocks
98 are Phanerozoic. In most deposits studied, the timing of gold mineralization is slightly younger than the age of the
99 country rocks, with the exception of the Rosebel deposit where the country rocks are Archean, whereas mineralization
100 formed during the Proterozoic (Daoust et al. 2011). Mineralization styles vary from quartz-carbonate veins to
101 replacement or disseminated. Tourmaline from Young-Davidson is from deformed, late, V3 quartz veins with low gold
102 contents (Martin 2012; Zhang et al. 2014). In the sample from Hira Buddini, tourmaline is part of the first tourmaline
103 stage that formed during amphibolite-facies metamorphism with the most significant gold mineralization event
104 (Hellmann et al. 2005; Krienitz et al. 2008).

105 Samples analyzed from other geological environments include metamorphic tourmaline from the Tehery-Wager area
106 (Canada; Steenkamp et al. 2016), hydrothermal tourmaline from veins cutting the LaRonde VMS deposit (Canada), and
107 tourmaline from Li-Cs-Ta-rich pegmatite associated with the Roberto gold deposit (Canada; Ravenelle et al. 2010;
108 Ravenelle 2013). The pegmatite emplacement at Roberto is associated with late D2, early D3, deformation that
109 postdates the metamorphism that affected the bulk of the gold mineralization. However, rare gold occurs within these

110 pegmatitic dikes (Ravenelle et al. 2010; Dubé et al. 2011; Ravenelle 2013; Fontaine et al. 2015). Additional samples
111 include tourmaline from the Lincoln Hill gold deposit in the Humboldt Range (Nevada, USA) that has epithermal
112 characteristics (R. Taylor, pers comm, 2015).

113 **Analytical methods**

114 **Sample selection**

115 Forty-nine polished thin sections from orogenic gold deposits and eight additional polished thin sections of tourmaline
116 from various geological settings were investigated using the petrographic microscope. One to 24 samples per deposit
117 were studied (Table 1). Samples were selected to represent textural, spatial and paragenetic variability within some
118 of the deposits. Deposits investigated using one sample yield limited variability for that deposit. The range of geological
119 characteristics of the selected deposits, however, is considered to be adequate to capture the compositional variability
120 of tourmaline in orogenic gold deposits, as shown for other minerals such as scheelite (Sciuba et al. 2020). This
121 assumption, however, constrains the data interpretation. In addition, even if tourmaline is from gold-bearing samples,
122 the paragenetic relation of tourmaline to gold is not known if gold was not found in the investigated samples. This
123 limitation is not critical as the study's objective is to define the chemical composition of tourmaline in gold-bearing
124 veins for indicator mineral surveys.

125 **Electron Probe Micro-Analysis (EPMA)**

126 Major and trace elements in tourmaline were measured with a CAMECA SX-100 Electron Probe Micro-Analyzer at
127 Université Laval using the analytical methods described in Grzela (2017). Analytical parameters were fixed at 10 µm
128 beam size, 15 kV voltage and 20 nA current. Major and minor element distributions were mapped using a 25 kV
129 voltage, 100 nA current and 20 ms dwell time per pixel. Following standards were used for calibration: hematite for
130 Fe, chromite for Cr, diopside for Ca, albite for Na, forsterite for Mg, quartz for Si, cordierite for Al, rhodochrosite for
131 Mn, rutile for Ti, orthoclase for K, sphalerite for Zn, chalcopyrite for Cu, nickeline for Ni, Co-ATX for Co, V-ATX for V,
132 Sc-ATX for Sc, tugtupite for Cl, celestite for Sr and, fluorite for F. Tourmaline structural formulae were calculated from
133 the EPMA data using an Excel spreadsheet based on the data reduction scheme in Henry et al. (2011). Tourmaline
134 major element composition was normalized to 29 oxygens and the structural formula was calculated based on 3 apfu
135 B and 4 apfu OH.

Laser Ablation-Inductively Coupled Plasma-Mass Spectrometry (LA-ICP-MS)

136
137 Minor and trace elements were measured with a RESolution M-50 Excimer 193 nm laser coupled to an Agilent 7700x
138 ICP-MS at the LabMaTer Laboratory at Université du Québec à Chicoutimi (Canada) using a frequency of 20 Hz and
139 fluence of 3 J.cm⁻². Line analyses were performed with a 33-44 µm beam size; spot analyses used a 55 µm beam size.
140 Backgrounds were measured for 30 s and tourmaline grains were ablated for 40-90 s. Maps of tourmaline trace
141 element concentration were generated using a 15 µm beam size with 20 s backgrounds between each ablating line.
142 ²⁹Si was used as an internal standard and fixed at 16.72 wt% based on the average Si measured by EPMA (16.72 ± 0.66
143 wt. %). Silicon shows the lowest variance in tourmaline in this study (Fig. 3). The reference materials NIST-610, GSD-
144 1g and GSE-1g were used as external standards for data quantification depending on the element (ESM 1 Table T1).
145 NIST-610, NIST-612, GSD-1g, GSE-1g and Gprobe6 were used as secondary standards to control data quality. All
146 reference materials are basalt glass. Data were extracted with Iolite software. Detection limits were calculated using
147 Longerich et al. (1996) and are reported in ESM 1 Table T1. The rim signal was commonly a mixed result of the
148 tourmaline rim and surrounding matrix and the rim area was too small to yield good quality data. Analyses of
149 inclusions and cracks were excluded in data integration.

Multivariate statistical analysis

150
151 EPMA and LA-ICP-MS data were investigated using Partial Least Square-Discriminant Analysis (PLS-DA; Makvandi et
152 al. 2016b). PLS-DA is a supervised statistical method that combines both Principal Component Analysis (PCA) and
153 linear regression. PLS-DA generates a series of orthogonal components that relate the X (N x K) and Y (N x M) matrices
154 by maximizing the covariance between matrices, and uses labeled data to enhance classification (de Iorio et al. 2007).
155 In the qw* loadings plot, elements that plot close to the origin do not covary, whereas those far from the center of the
156 plot show strong covariations. Elements that plot in opposite quadrants have inverse covariations. Elements that
157 explain the compositional variance of a class of samples, such as a deposit type, plot close to the class label or in the
158 opposite quadrant if they covary inversely. In scores (t) diagrams, samples plotting near a data class label have similar
159 compositional characteristics. The Variable Importance on Projection (VIP) measures the importance of an element in
160 the classification (Eriksson et al. 2001), such that VIP values that are equal or larger than 1 are the most significant for
161 the classification (Eriksson et al. 2001). Prior to multivariate statistical analysis, EPMA and LA-ICP-MS data were
162 transformed using centered-log ratio (Aitchison 1986; Whitten 1995), suitable for multivariate statistical analysis
163 (Aitchison 1986; Egozcue et al. 2003; Thió-Henestrosa and Martín-Fernández 2005; Makvandi et al. 2016b). Censored

164 values were imputed by the R-package robCompositions using the k-nearest neighbor function (Hron et al. 2010) as
165 described in Makvandi et al. (2016a) and Sciuba et al. (2020). Elements with more than 40 % concentrations below
166 detection limit were excluded from the multivariate analysis.

167 **Results**

168 **Tourmaline textures and mineral assemblages**

169 In orogenic gold deposits, tourmaline is commonly found in quartz-carbonate veins or disseminated in country rocks.
170 Tourmaline presents a wide range of sizes (μm to cm), textures, colors, optical zoning and mineral associations. The
171 petrographic characteristics of tourmaline from investigated orogenic gold deposits are summarized in Table 2.
172 Tourmaline forms aggregates of fine grained (μm scale) anhedral crystals in some deposits (e.g. Hoyle Pond, Canadian
173 Malartic, James Bay, Rosebel, Salsigne, Hira Buddini). In others, aggregates of tabular to acicular euhedral, medium
174 size grains (e.g, Essakane, New Consort, St. Ives, mm scale; Fig. 1) predominate. Under plane-polarized light, the most
175 common tourmaline color in orogenic gold deposits is bluish-green to brown. In some cases, tourmaline is light blue
176 or orange. Tourmaline typically shows rims with colors from orange to brown to dark green, with thickness up to 50
177 μm (Fig. 1). In orogenic gold deposits, rare complex grains exhibit oscillatory zoning, patchy and/or sector zoning (Fig.
178 2). Tourmaline is commonly associated with quartz, calcite, ankerite, dolomite, biotite, sericite, K-feldspar, rutile,
179 magnetite, pyrite, arsenopyrite, pyrrhotite, chalcopyrite and gold (Fig. 1). In the samples from Rosebel and Essakane,
180 tourmaline textures suggest co-precipitation with gold (Fig. 1f). At Hoyle Pond and St. Ives, tourmaline occurs with
181 native gold but not in contact. In some deposits, a single generation of tourmaline is associated with mineralization
182 but in rare cases such as at Roberto, two generations of tourmaline are present. Subhedral orange tourmaline is found
183 within ferro-magnesian greywacke and with disseminated gold mineralization. Anhedral brown tourmaline occurs in
184 the selvage of mineralized quartz-diopside veins or in hydrothermal breccias in greywacke (Fontaine et al. 2015).
185 Tourmaline may contain inclusions of quartz (Hoyle Pond, Young Davidson, Roberto, James Bay, Rosebel, New Consort,
186 Uti, St. Ives), calcite (Canadian Malartic), chlorite (Rosebel), or amphibole (Roberto). Fractures in tourmaline are filled
187 with quartz (James Bay, Roberto, Lincoln Hill, Essakane), chlorite (Canadian Malartic, James Bay, Salsigne), calcite (St.
188 Ives) or pyrrhotite (New Consort; Fig. 1). In the Roberto pegmatite, tourmaline is coarse grained (up to 4.5 mm),
189 anhedral to subhedral, and is associated with quartz and microcline.

190 **Major element compositions**

191 Major and minor element compositions of tourmaline measured by EPMA shows large compositional ranges in Al, Fe,
192 and Mg (Fig. 3; ESM 1 Table T2). Calcium, Ti, and V show large standard deviation caused by chemical zoning (Figs. 3a
193 and 4). Tourmaline from orogenic gold deposits plots most commonly in the alkali group (Fig. 5a). Rare examples from
194 Salsigne, Rosebel, Hoyle Pond and the James Bay district plot in the X-vacant group, but have compositions close to
195 those within the alkali group (Fig. 5a). Tourmaline from orogenic gold deposits has dravite to, less commonly, schorl
196 composition (Fig. 5b and c). Minor exceptions from James Bay, Big Bell and Hoyle Pond show magnesio-foitite
197 compositions; some tourmaline grains from Salsigne, New Consort and Rosebel plot in the foitite field. Orange
198 tourmaline from Roberto is dravite, whereas most brown tourmaline from Roberto is schorl (Fig. 5b). In the
199 Mg/(Fe+Mg) vs Ca/(Ca+Na) diagram, brown tourmaline from Roberto shows uvite and feruvite compositions (Fig. 5c).
200 PLS-DA with major elements does not reveal any group discrimination on mineralization age, country rock
201 composition, and local metamorphic facies (ESM 2 Fig. S2). Tourmaline from the Lincoln Hill gold deposit, the
202 hydrothermal veins cutting the VMS mineralization at LaRonde, and from the Tehery Wager area, also belongs to the
203 alkali group (Fig. 5a).

204 **Minor and trace element composition**

205 A total of 253 line and four spot analyses were performed in areas free of mineral inclusions as verified by petrographic
206 observations (ESM 1 Table T3). EPMA and LA-ICP-MS data show strong covariation for Na, K, Fe, Al, Mg, Mn, Ni, Zn and
207 V (Fig. 3; ESM 2 Fig. S1). Covariation is weaker for Ca, Ti and Sc reflecting chemical zoning (ESM 2 Fig. S1). Blue
208 tourmaline is characterized by low Ti contents (median= 0.10 wt %) compared to orange tourmaline (median= 0.44
209 wt %), and brown tourmaline (median= 0.40 wt %; ESM 2 Fig. S3). Pearson correlation coefficient r shows moderate
210 to strong covariation (0.40 to 0.97) for High Field Strength Elements (HFSE: Zr, Hf, Nb, Ta, Y, REE, Th and U), Large Ion
211 Lithophile Elements (LILE: K, Ba), and several highly compatible transition metals (Ti, Cr, V, Co and Ni; Fig. 6; ESM 2
212 Table T4; ESM 2 Figs. S4 and S5). Gallium and Sn show broad increase with increasing metamorphic facies of the
213 country rock and from mafic to felsic rocks (Table 3; Fig. 6e and i; ESM 2 Figs. S4 and S5). Tourmaline from deposits
214 hosted in lower greenschist to lower amphibolite facies sedimentary rocks has intermediate Ga and Sn concentrations
215 (median= 32.6 and 1.31 ppm, respectively). Canadian Malartic is an exception where tourmaline has Ga concentrations
216 (median 69.8 ppm) similar to those of lower greenschist to lower amphibolite facies felsic rocks, but intermediate Sn
217 concentration (median 2.11 ppm; Table 3). Iron and Sn correlate moderately ($r = 0.57$) in tourmaline from deposits

218 hosted in lower greenschist to lower amphibolite terrains (Fig. 6e). Tourmaline hosted in middle to upper amphibolite
219 facies rocks tends to have higher concentrations of Hf, Nb, Ta, Y, U, Th, and Ti than that from deposits hosted in lower
220 greenschist to lower amphibolite facies rocks (Table 3, Fig. 6, ESM 2 Figs. S4 and S5). Tourmaline from deposits hosted
221 in middle to upper amphibolite facies rocks has higher \sum LREE (median= 11.05 ppm) compared to that from deposits
222 hosted in lower greenschist to lower amphibolite facies rocks (median= 0.55 ppm \sum LREE; Table 3, ESM 2 Fig. S6).
223 Rare earth elements patterns for each deposit are presented in ESM 2 Fig. S9. Tourmaline from orogenic gold deposits
224 displays three REE patterns (Fig. 7, ESM 2 Figs. S6 and S9): 1) a HREE-enriched with $(La/Yb)_{CN}$ ratios less than 0.1
225 (ESM 2 Fig. S6a); ESM 2 Fig. S9); 2) a LREE-enriched pattern with $(La/Yb)_{CN}$ ratio greater than 10 and positive Eu
226 anomaly; and 3) a flat pattern with $(La/Yb)_{CN}$ ratios between 0.1 and 10 and positive Eu anomaly (ESM 2 Figs. S6a and
227 S9f, i and j). The LREE-enriched and flat patterns are the most common in tourmaline from orogenic gold deposits.
228 Tourmaline from deposits hosted in felsic rocks tends to have a smaller Eu anomaly (median $Eu^* = 2.02$) compared to
229 those from deposits within in mafic and sedimentary rocks (median $Eu^* = 4.6$ and 15.1 , respectively, Fig. 8b). The REE
230 patterns of tourmaline from orogenic gold deposits do not correlate with the composition and metamorphic facies of
231 the country rocks, or mineralization age.
232 In some tourmaline grains, two REE patterns are present (ESM 2 Fig. S10). At St. Ives, a bluish-grey tourmaline core is
233 characterized by a HREE-enriched pattern, whereas the greenish brown rim has a LREE-enriched pattern (ESM 2 Fig.
234 S10a). In contrast, tourmaline from Rosebel, with similar textures and colors than that of St. Ives, has LREE-enriched
235 patterns in both rim and core (ESM 2 Fig. S10b). No systematic relationship exists between REE pattern, texture, color
236 and zoning in tourmaline from orogenic gold deposits.
237 Tourmaline from hydrothermal veins cutting the VMS mineralization at LaRonde and from the Lincoln Hill gold deposit
238 has REE patterns similar to those of tourmaline from orogenic gold deposits, with LREE-enriched and flat REE patterns
239 with positive Eu anomalies (ESM 2 Fig. S11a and b). Tourmaline from the Roberto pegmatite displays three REE
240 patterns (ESM 2 Figs. S11c and S12): (1) flat with a large negative Eu anomaly ($(La/Yb)_{CN} \sim 2.1$; $Eu^* \sim 0.02$), (2) weakly
241 LREE-enriched with a moderate negative Eu anomaly ($(La/Yb)_{CN} \sim 8.8$; $Eu^* \sim 0.4$), and (3) a strongly LREE-enriched
242 with a small negative Eu anomaly ($(La/Yb)_{CN} \sim 99.8$; $Eu^* \sim 0.6$), that show inconsistent relation to color zoning (ESM
243 2 Fig. S12).

244 **Chemical zoning**

245 Core and rim of the same tourmaline grain commonly have similar major element compositions such that they plot
246 close to each other in the classification diagrams (Fig. 5). EPMA and LA-ICP-MS maps of tourmaline show that zoning

247 is systematically characterized by variations in Ti, V, Co, Cr, Ni and Sc, whereas Si, Al and Na show small variations
248 (Fig. 4). Iron and Mg vary with zoning in James Bay area tourmaline (Fig. 4) but not systematically in other deposits
249 (ESM 2 Fig. S7). Variations are not systematic, however. Excelsior tourmaline core has a higher V concentration than
250 the rim, in contrast to tourmaline from Rosebel where the core has lower V than the rim (ESM 2 Fig. S7). Tourmaline
251 from Hoyle Pond is Ti-poor in the core but Ti-rich in the rim, in contrast to Excelsior where the core is Ti-rich and the
252 rim is Ti-poor (ESM 2 Fig. S7). EPMA and LA-ICP-MS maps reveal complex micrometric-scale concentric zoning in
253 some tourmaline characterized by variations in Fe, Mg, Ca, Mn, K, Ga, Sr, and Li concentrations that are not related to
254 the color variation under polarized light (Figs. 2 and 4).

255 **Multi-variate analysis of tourmaline composition in relation to geological environment**

256 Partial Least Square-DA includes tourmaline data with the same set of compositional data from the Val-d'Or (Grzela et
257 al. 2019) and Meliadine (Manégliá et al. 2018) gold districts . LA-ICP-MS results for major, minor and trace elements
258 were classified by country rock composition, simplified as the main country rock type (Table 1; Fig. 9), metamorphic
259 facies of the country rocks (Table 1; Fig. 10), and age of gold mineralization, simplified by geological period (Table 1,
260 ESM 2 Fig. S8).

261 Country rock compositions define qw^*_1 by moderate positive contributions of Sc, Co, Yb and Lu and large negative
262 contributions of Eu, Li, Mn, Ti and Ca (Fig. 9a). In contrast, qw^*_2 is defined by large positive contributions of Sr and Ga
263 and negative contributions of Eu, Al, B and Li (Fig. 9a). Tourmaline from orogenic gold deposits hosted in sedimentary
264 rocks commonly has negative t_1 scores caused by Eu, Li, Mn, Ti (VIP >1.5) and negative to positive t_2 scores (Fig. 9b
265 and c). Tourmaline from deposits hosted in felsic rocks typically has positive t_1 and t_2 scores caused by covariations of
266 Sr, Eu and Ga (VIP >1.5). Tourmaline from deposits hosted in intermediate composition rocks has positive t_1 scores
267 and t_2 scores close to 0, as a result of covariations of Pb, Cu, Ni and, Li (VIP >1.5). Tourmaline from deposits hosted in
268 mafic rocks commonly has positive t_1 and negative t_2 scores, caused by Sr, Eu and, Ga (VIP >1.5; Fig. 9). In summary, t_1
269 discriminates tourmaline hosted by sedimentary rocks from that hosted by felsic to mafic rocks, whereas t_2 classifies
270 the country rocks from felsic to mafic, with overlap between the different rock types.

271 Country rock composition and metamorphic facies yield qw^*_1 defined by positive contributions of Fe and Na and
272 negative contributions of La, Eu, Mn, Sn and Li, whereas qw^*_2 is defined by positive contributions of Lu and Yb and
273 negative contributions of Al, Li, B, Eu, Mn, Mg, Ti and Ca (Fig. 10a). In the t_1 - t_2 plot (Fig. 10b), tourmaline hosted in
274 lower greenschist to lower amphibolite facies rocks plot at low t_1 and t_2 scores caused by covariations of Ca, Sr and Eu
275 that have VIP values greater than 1 (Fig. 10b, c). Tourmaline from deposits hosted in middle to upper amphibolite

276 facies rocks is characterized by negative t_1 scores as a result of covariations between Li, Na, Al, Ca, Mn, Fe, La, and Eu,
277 and by negative to positive t_2 scores (Fig. 10b).

278 Country rock composition and deposit age yields qw^*_1 defined by positive contributions of Sc, Fe, Co and Na and
279 negative contributions of Ca, La, Ti, Mn, Li and Eu, whereas qw^*_2 is defined by positive contributions of Lu, Yb and Y
280 and negative contributions of Zn, Al and Eu (ESM 2 Fig. S8a). Tourmaline from Archean orogenic gold deposits spreads
281 across negative to positive t_1 and t_2 scores (ESM 2 Fig. S8b). Tourmaline from Proterozoic deposits has t_1 scores close
282 to 0 and negative to positive t_2 scores, overlapping with Archean deposits. Phanerozoic tourmaline from the Excelsior
283 deposit has positive t_1 and t_2 scores caused by Zn, Sr, Ga and, Eu (VIP >1.5; ESM 2 Fig. S8c).

284 **Discussion**

285 **Influence of geological settings**

286 Major and trace element composition of tourmaline vary with several factors including coexisting minerals (Taylor
287 and Slack 1984; Griffin et al. 1996; Slack et al. 1999; Grzela 2017), fluid composition (Slack and Trumbull 2011) and
288 physical conditions during crystallization, including P-T regimes and oxygen fugacity (Dutrow and Henry 2011; Van
289 Hinsberg 2011). PLS-DA results show that tourmaline from orogenic gold deposits lacks compositional variation with
290 age of mineralization, in contrast to scheelite (Sciuba et al. 2020; ESM 2 Fig. S8). The major element composition of
291 tourmaline is known to be influenced by that of the host rocks (Henry and Guidotti 1985; Lottermoser and Plimer
292 1987; Slack and Coad 1989; Gallagher and Kennan 1992; Slack 1996; Slack 2002; Van Hinsberg and Schumacher 2011;
293 Berryman et al. 2017). However, PLS-DA for major elements do not discriminate samples by country rock composition
294 (ESM 2 Fig. S2). Slack and Coad (1989) highlighted that in systems with high fluid/rock ratios, such as shear zones and
295 veins, typical of orogenic gold deposits (Goldfarb et al. 2005), major elements in tourmaline are buffered by the fluid
296 phase.

297 Van Hinsberg (2011) showed that magmatic tourmaline does not significantly fractionate trace elements from silicate
298 melt, and that trace element incorporation under these conditions follows rules of lattice-strain theory. Thus, the trace
299 element variations in relation to optical zoning in orogenic gold deposit tourmaline could record variable fluid
300 compositions. Others, such as Galbraith et al. (2009) and Hazarika et al. (2015), noted that high Co and Ni
301 concentrations in tourmaline from the Tsa da Glisza emerald prospect and the Hutti and Hira-Buddini gold deposits
302 correlate with the presence of mafic protoliths. Tourmaline from orogenic gold deposits hosted in mafic rocks tend to
303 have high Ni and Co concentrations, but this is not systematic (Fig. 6h). King (1988) and King and Kerrich (1989)

304 reported that tourmaline from the Timmins-Porcupine orogenic gold district, hosted in ultramafic rocks, is
305 characterized by high Cr and Mg concentrations. Jiang et al. (2004) proposed that Rb and Cs, Sr and transition metals
306 Mn, Sc, V, Co, Cr and Ni contents in tourmaline reflect concentrations of these elements in the host rocks. In orogenic
307 gold deposits, Ga and Sn are the only trace elements in tourmaline that show systematic variation with country rock
308 composition (Fig. 6i; ESM 2 Figs. S4a and S5d). In deposits hosted by lower greenschist to lower amphibolite facies
309 rocks, Ga and Sn concentrations are high in felsic rocks and low in mafic rocks, consistent with the incompatible
310 behavior of Ga and Sn during magmatic differentiation. The intermediate Ga and Sn concentrations in tourmaline from
311 deposits hosted in sedimentary rocks likely reflect compositional heterogeneity of the sedimentary source. Canadian
312 Malartic is dominantly hosted by clastic sedimentary rocks, but the tourmaline analyzed is from a mineralized vein
313 within a monzodiorite dike, consistent with its signature similar to that of tourmaline hosted in felsic rocks. Other
314 binary diagrams do not reveal strong correlations in trace element compositions of tourmaline with that of the country
315 rock compositions (Fig. 6, ESM 2 Figs. S4 and S5). PLS-DA of trace elements, however, yields a good classification based
316 on country rock composition, in which tourmaline hosted in sedimentary rocks have negative t_1 in contrast to positive
317 t_1 for tourmaline within mafic to felsic rocks, which are further classified by t_2 according to magmatic differentiation
318 (Fig. 9b). The overlap among the different country rock composition classes, defined by the composition of the
319 dominant lithology in the rock package hosting the orogenic gold deposits (Fig. 9b) indicates that tourmaline records
320 the trace element signature of the country rocks, as a result of fluids sourced from the regional country rocks or of
321 fluid-rock exchange during flow.

322 Tourmaline from orogenic gold deposits hosted in middle to upper amphibolite facies rocks, irrespective of country
323 rock composition, commonly have higher concentrations of Ti, Ga, Sn, Σ REE, Zr, Hf, Nb, Ta, Th and U compared to those
324 from deposits within lower greenschist to lower amphibolite facies rocks (Fig. 6, ESM 2 Figs. S4 and S5). Rutile is
325 typically an accessory mineral in gold mineralization hosted in lower greenschist to lower amphibolite facies rocks. At
326 middle to upper amphibolite facies, rutile is absent from the characteristic mineral assemblages of orogenic gold
327 deposits (Eilu et al. 1999). Zack et al. (2002) showed that rutile strongly partitions HFSE, which perhaps explains the
328 higher concentrations of Ti, Ga, Sn, and HFSE within these tourmalines in absence of rutile at higher metamorphic
329 facies. Other minerals such as xenotime, apatite or scheelite may also scavenge these trace elements (Belousova et al.
330 2002; Kositcin et al. 2003; Mao et al. 2016; Sciuba et al. 2020). However, they occur in orogenic gold mineralization
331 independently of host rock composition and metamorphic facies (McCuaig and Kerrich 1998; Vielreicher et al. 2003;
332 Sciuba et al. 2020), which is unlikely to explain the trace element distribution in tourmaline from orogenic gold

333 deposits hosted in higher metamorphic grade. Trace elements in coexisting rutile, xenotime and apatite have not been
334 measured in our samples, such that we cannot discuss partitioning in detail.

335 **Rare Earth Elements**

336 Orogenic gold systems fluid is dominated by sulfide complexes and has low salinity with 3-7 wt.% NaCl (Kerrick 1993;
337 Goldfarb and Groves 2015). In these fluids, REE are likely transported as sulfide complexes, with similar solubilities at
338 all temperatures (Migdisov et al. 2016). Thus, the high LREE and low HREE contents in tourmaline hosted in middle
339 to upper amphibolite facies country rocks (ESM 2 Fig. S6) are unlikely caused by fractionation during hydrothermal
340 precipitation. At middle amphibolite facies, garnet appears in the mineral assemblage associated with gold
341 mineralization (Eilu et al. 1999). Garnet is characterized by HREE-enriched patterns (Rubatto 2002), which could
342 explain the HREE-depleted tourmaline in the Big Bell deposit, where almandine and andradite occur in close
343 association with massive quartz-tourmaline veins (Mueller et al. 1996). Garnet is absent in the mineral assemblage of
344 gold mineralization at the Roberto deposit (Fontaine et al. 2014), which is consistent with lack of HREE depletion in
345 tourmaline.

346 Jiang et al. (2004) suggested that the HREE-enriched patterns in tourmaline from the Yunlong Sn deposit are caused
347 by REE-rich mineral inclusions such as zircon, xenotime, monazite or allanite in tourmaline. Hazarika et al. (2015) also
348 noted positive covariations between Σ REE and Ti, Y, and Zr, and attributed HREE-enriched patterns to zircon or
349 titanite inclusions that would be invisible via optical microscope and SEM. However, there were no Zr or Ti spikes in
350 the LA-ICP-MS signal, thus suggesting lack of inclusions in the analyzed tourmaline. Samples with HREE-enriched
351 patterns (Hoyle Pond and Excelsior) have Y, Zr, Ca and Ti contents similar to those in tourmaline with other types of
352 REE patterns (Fig. 6; ESM 2 Figs. S4, S5 and S6). Titanium and Ca contents, measured along trenches (~ 33-44 μ m wide
353 x 100 μ m long) by LA-ICP-MS, are similar to those measured via 10 μ m spots by EPMA (Fig. 3 and ESM 2 Fig. S1b and
354 j). Tourmaline with HREE-enriched pattern, however, could form from fluids that dissolved HREE-rich minerals as
355 suggested by Migdisov et al (2009).

356 The diverse REE patterns documented in tourmaline from orogenic gold deposits (Fig. 7; ESM 2 Fig. S9) were
357 previously recognized in tourmaline from other types of mineral deposits and geological settings (Jiang et al. 2002;
358 Jiang et al. 2004; Roberts et al. 2006; Roda-Robles et al. 2015; Harlaux 2016; Iveson et al. 2016; Berryman et al. 2017;
359 Hazarika et al. 2017; Kalliomäki et al. 2017; Harlaux et al. 2018; Manégliä et al. 2018; Wang et al. 2018; Grzela et al.
360 2019), and thus are not discriminant of deposit types or geological environments.

361 **Comparing tourmaline from various deposit types and geological environments**

362 The trace element composition of tourmaline from orogenic gold deposits is compared with those from other deposit
363 types and geological settings from literature (Figs. 11 and 12, ESM 2 Figs. S13 and S14). Vanadium correlates
364 moderately with Ni ($r=0.55$), Nb with Ta ($r=0.58$), Zr with Y ($r=0.39$) and, Th with U ($r=0.75$) in tourmaline from all
365 deposit types and geological settings (Figs. 11 and 12, ESM 2 Figs. S13 and S14), similarly to tourmaline from orogenic
366 gold deposits (ESM 2 Table T4). Literature data for tourmaline from orogenic gold deposits (King et al. 1988; Koval et
367 al. 1991; Jiang et al. 2002; Deksisa and Koeberl 2004; Roberts et al. 2006; Hazarika et al. 2015; Hazarika et al. 2016;
368 Grzela 2017; Manégliá 2017) plot with tourmaline from this study in binary and PLS-DA plots (Figs 8, 11 and 12, ESM
369 2 Figs. S13 and S14). Thus, we discuss all orogenic gold deposits tourmaline data together.

370 Tourmaline from orogenic gold deposits has a compositional range similar to that of tourmaline from various deposit
371 types and geological settings for Ti, Zn, K, Cr, Sc, Co, Cu, Mn, Pb, Zr, Y and Rb (Figs 3, 11 and 12, ESM 2 Figs. S13 and
372 S14). As a result, data for these elements are not useful for discriminating orogenic gold deposits from other deposit
373 types. Tourmaline from orogenic gold deposit contains higher V, Sr and Ni concentrations (median 398 ppm V, 437
374 ppm Sr, 38 ppm Ni) compared to tourmaline from other magmatic-hydrothermal (median 160 ppm V, 78 ppm Sr, 11
375 ppm Ni) and magmatic environments (median 25 ppm V, 8 ppm Sr, 5 ppm Ni; Fig 11 and ESM 2 Fig. S13 and Fig. S14).
376 Tourmaline from magmatic-hydrothermal deposits, including porphyry Cu-Mo, W-(Sn) veins, Sn skarns, Sn deposits
377 and veins, commonly has intermediate concentrations of V and Sr, whereas Ni concentrations are similar to those in
378 tourmaline from pegmatites and granites. Tourmaline from orogenic gold deposits has low Li, Be, Ga, Sn, Nb, Ta, U and
379 Th concentrations compared to tourmaline from magmatic-hydrothermal and magmatic environments (Fig 11, ESM 2
380 Figs. S13 and S14). Tourmaline from the Lincoln Hill gold deposit has V, Sr, Nb and Sn concentrations (median 79 ppm
381 V, 523 ppm Sr, 0.15 ppm Nb, 3.81 ppm Sn) between those of orogenic gold deposits and magmatic-hydrothermal
382 environments, but which plot mostly with orogenic gold deposits in binary diagrams (Fig. 11, ESM 2 Figs. S13 and
383 S14). Tourmaline from hydrothermal veins that cut VMS mineralization at LaRonde (Canada) plots in the orogenic
384 gold deposit field in binary plots (Figs. 8 and 11, ESM 2 Figs. S13 and S14). Those veins are not considered auriferous
385 (D. Pitre, pers comm, 2015), but likely formed during the same hydrothermal event that produced the orogenic gold
386 deposits in the Abitibi subprovince. This indicates that the geochemical signature of the regional country rocks
387 dominates over that of the local VMS rock composition.

388 Ratios combining an element characterized by a high concentration in tourmaline from orogenic gold deposits such as
389 V, Sr and Ni, over an element with a low concentration, such as Li, Be, Ga, Sn, Nb and Ta efficiently separate tourmaline

390 of different origins. For example, tourmaline from orogenic gold deposits has relatively high Zn/Nb, Co/Nb and, Sr/Ta
391 ratios compared to tourmaline from magmatic-hydrothermal and magmatic environments, such that binary diagrams
392 using Sr/Li vs V/Sn, Sr/Sn vs V/Nb, Sr/Sn vs Ni/Nb and Sr/Sn vs V/Be are efficient in discriminating tourmaline from
393 orogenic gold deposits from those from other deposit types and environments (Fig. 11, ESM 2 Figs. S13h and S14).

394 Tourmaline compositions from orogenic gold deposits is compared with those from various deposit types and
395 geological settings using PLS-DA (Fig. 12). Literature contains sufficient data for Li, Sc, V, Co, Zn, Sr, Sn and Pb only.
396 The PLS-DA analysis yields qw^*_1 defined by positive contributions of V and Sr and negative contributions of Li and Sn,
397 whereas qw^*_2 is defined by positive contributions of Co and Pb and negative contributions of Sc and Zn (Fig. 12a). Data
398 for tourmaline from orogenic gold deposits plot in a separate field with positive t_1 , and negative to positive t_2 scores
399 caused by covariations of V, Sr, Sn and Li (VIP >1; Fig. 12c). Tourmaline from unmineralized metamorphic
400 environments has positive to negative t_1 and t_2 defined by Sc, Co and Pb covariations (VIP >1; Fig. 12c). Tourmaline
401 from the Lincoln Hill gold deposit has low positive t_1 and negative t_2 scores such that the results plot with the orogenic
402 gold deposits, close to the magmatic-hydrothermal field (Fig. 12b), similar to binary diagrams (Fig 11, ESM 2 Figs. S13
403 and S14). Taking into account that tourmaline is an uncommon mineral in epithermal gold deposits and that its
404 composition in that deposit type has not been investigated, we suggest that the Lincoln Hill deposit affinity may need
405 to be re-evaluated. Tourmaline from the other hydrothermal deposits, including polymetallic Pb-Zn-Cu±U veins and
406 Sn-Pb-Zn stratiform deposits, has negative t_1 and positive t_2 scores defined by covariations of Zn and Pb (VIP >1; Fig.
407 12c). Tourmaline from magmatic environments, including pegmatites and granites, has negative t_1 and positive to
408 negative t_2 scores caused by moderate covariations of Sn, Li, Sr and V (VIP >0.8; Fig. 12c). Tourmaline from the Roberto
409 pegmatite plots close to the orogenic gold field (Fig. 12b), suggesting that this tourmaline may have formed from fluids
410 similar to those from orogenic gold deposits. Tourmaline from magmatic-hydrothermal environments has negative t_1
411 and positive to negative t_2 scores caused by moderate covariations of Zn, Pb, Sn, Co and Sc (VIP >0.8; Fig. 12c). PLS-
412 DA, thus shows that tourmaline from various deposit types and environments is effectively discriminated by qw^*_1 and
413 that the trace elements that define qw^*_1 , including Sr, V, Sn and Li, efficiently discriminate tourmaline from orogenic
414 gold deposits from those of other deposit types and geological environments.

415 The low variance of orogenic gold tourmaline composition, as shown in binary diagrams and PLS-DA (Figs 8, 11 and
416 12, ESM 2 Figs. S13 and S14), is consistent with the low geochemical variance of the hydrothermal fluid composition
417 that formed the orogenic gold mineralization (Goldfarb and Groves 2015). Goldfarb and Groves (2015) proposed that
418 this low compositional variance of the hydrothermal fluid reflects a single source located at upper to middle crustal

419 depth. However, the trace element compositional variation of tourmaline from orogenic gold deposits indicates that
420 the primary hydrothermal fluid composition varies with the regional lithological packages. This dichotomy suggests
421 that some elements (e.g. Nb, Ta, U, Th) are derived from the primary crustal source, whereas others (e.g. Ni, V, Ga, Sn)
422 are derived from reaction between the fluids and local country rocks, as suggested by Goldfarb and Groves (2015).
423 Binary diagrams and PLS-DA results show a transition in the trace element composition of tourmaline from orogenic
424 gold to hydrothermal, to magmatic-hydrothermal deposits and then, to magmatic environments (Figs. 11 and 12, ESM
425 2 Figs. S13 and S14). This gradation in composition likely reflects the broad transition between fluids sourced from
426 prograde metamorphism of country rocks to hydrothermal fluids equilibrated with crustal rocks with increasing
427 magmatic fluid contributions and then, to LREE-enriched magmatic environments.

428 Marks et al. (2013) highlighted that the trace element composition of tourmaline in granite is expected to reflect the
429 trace element behaviour during fractional crystallization and partial melting, such that incompatible elements, such
430 as LILE (e.g. Li, Be) and HFSE (e.g. Nb, Ta, U, Th), that are concentrated in the residual melt, are enriched in tourmaline
431 associated with highly evolved granite and pegmatite. Tourmaline from orogenic gold deposits has high Ni and V and
432 low Li, Be, Ga, Sn, Nb, Ta, U and Th concentrations compared to tourmaline from magmatic and magmatic-
433 hydrothermal environments (Fig. 12g). Ultramafic and mafic igneous rocks are commonly part of the regional country
434 rock package hosting orogenic gold deposits (Goldfarb et al. 2005), which may explain the high concentrations of
435 compatible Ni and V, and the low concentrations of incompatible Li, Be, Ga, Sn, Nb, Ta, U and Th in tourmaline from
436 orogenic gold deposits. In contrast, tourmaline in felsic magmatic rocks has low concentrations in Ni and V and high
437 concentrations in Li, Be, Ga, Sn, Nb, Ta, U and Th. Strontium is high in tourmaline from orogenic gold deposits compared
438 to magmatic and magmatic-hydrothermal environments. It has been proposed that Sr was derived from basement
439 rocks below the greenstone belt hosting the orogenic gold deposits (Kerrich 1989; Mueller et al. 1991) whereas in
440 other deposits, a local wallrock origin for both Sr has been proposed (Miller et al. 1995; Kempe et al. 2001). In contrast,
441 Böhlke and Kistler (1986) favored multiple strontium sources from the country rocks. Similarly, the covariation of
442 oxygen and strontium isotope composition in tourmaline from the Val-d'Or orogenic gold district was interpreted to
443 be the result of mixing between a deep-seated fluid that leached less radiogenic Sr from volcanic and sedimentary
444 country rocks, and an upper crustal fluid that had leached radiogenic Sr from plutonic, seawater-altered volcanic, or
445 Archean carbonate rocks (Beaudoin and Chiaradia 2016).

446 Tourmaline from VMS and SEDEX deposits (Griffin et al. 1996) has relatively high Ba concentrations that discriminate
447 these sources from tourmaline from orogenic gold deposits and magmatic-hydrothermal and magmatic environments

448 (Fig. 11e). Barium is high in VMS and SEDEX environments where barite is commonly part of the mineral assemblage
449 of the massive sulfides lenses in VMS deposits, and can form large bedded to massive accumulations in SEDEX deposits
450 (Leach et al. 2005). This pattern suggests that Ba can be used a discriminant element to differentiate tourmaline from
451 Ba-rich environments, such as VMS and SEDEX deposits.

452 **Conclusions**

453 Orogenic gold deposit tourmaline belong most commonly to the alkali group and has dravite to schorl compositions.
454 Major element compositions are independent of the composition and metamorphic facies of the country rocks.
455 However, our data show that Sn and Ga systematically vary with both of these parameters. Tin and Ga display similar
456 behavior with low concentrations in mafic rocks, high concentrations in felsic rocks, and intermediate concentrations
457 in sedimentary rocks. Tin and Ga both increase with increasing metamorphic grade of the country rocks. Tourmaline
458 from orogenic gold deposits hosted in middle to upper amphibolite facies rocks tends to have higher concentration of
459 HFSE including REE, Hf, Nb, Ta, Y, U and Th, as well as Ti, relative to those from deposits hosted in lower greenschist
460 to lower amphibolite facies rocks. Partial Least Square-DA results highlight a combination of several trace elements
461 that can discriminate the geological settings of the orogenic gold deposits including composition and metamorphic
462 grade of the country rock. Some elements such as Ga and Sn are derived from local country rocks whereas others such
463 as HFSE are probably derived from regional country rocks. Tourmaline from orogenic gold deposits displays three
464 different REE patterns including HREE-enriched, a LREE-enriched (most common), and flat. These three REE patterns
465 are documented in tourmaline from various deposit types and geological settings and are not diagnostic.
466 The trace element composition of tourmaline from orogenic gold deposits has a distinctive signature characterized by
467 high V, Sr and Ni and low Li, Be, Ga, Sn, Nb, Ta, U and Th concentrations compared to tourmaline from other deposit
468 types and geological settings. Binary plots including Sr/Li vs V/Sn, Sr/Sn vs V/Nb, Sr/Sn vs Ni/Nb and Sr/Sn vs V/Be,
469 as well as PLS-DA results, discriminate tourmaline from orogenic gold deposits from that from other deposit types and
470 geological settings. Tourmaline trace element composition reflects a transition in geological environments between
471 metamorphic, hydrothermal, magmatic-hydrothermal, and magmatic. Thus, tourmaline trace element compositions
472 have a great potential to constrain provenance in exploration using data from overburden sediments.

473 **Acknowledgements**

474 This research project was funded by the Natural Sciences and Engineering Research Council of Canada, Agnico Eagle
475 Mines Ltd, and the Ministère de l'Énergie et des Ressources Naturelles du Québec. We gratefully acknowledge people

476 and companies that provided samples for study: Aurico Gold (new: Alamos Gold), Clovis Auger (InnovExplo), Caroline
477 Daoust, S. De Souza (UQAM), Annika Dziggel (RWTH), Arnaud Fontaine (INRS-ETE), Richard Goldfarb (Goldfarb Global
478 Gold), Goldcorp, Roman Hanes (Université Laval), Andre Hellman (RWTH), Erin Marsh (USGS), Andreas Mueller
479 (UWA), David Pitre (Agnico Eagle), Louis Raimbault (École des Mines de Paris), Holly Steenkamp (Canada-Nunavut
480 Geoscience Office), and Ryan Taylor (USGS). M. Choquette (Université Laval), A. Ferland (Université Laval), D. Savard
481 (UQAC) and P. Pagé (UQAC) are thanked for technical assistance with EPMA, SEM and LA-ICP-MS analyses. We
482 gratefully thank J. Slack, M. Harlaux, R. Trumbull and Chief-Editor B. Lehman for their comments which improved
483 significantly the manuscript.

484 **References**

- 485 Aitchison J (1986) *The Statistical Analysis of Compositional Data*. Monographs on Statistics and Applied Probability.
486 London (UK)
- 487 Anglin CD, Jonasson IR, Franklin J (1996) Sm-Nd dating of scheelite and tourmaline: Implications for the genesis of
488 Archean gold deposits, Val d'Or, Canada. *Econ Geol* 91:1372-1382
- 489 Bačík P, Uher P, Ertl A, Jonsson E, Nysten P, Kanicky V, Vaculovic T (2012) Zoned REE-enriched dravite from a granitic
490 pegmatite in Forshammar Bergslagen province, Sweden; an EMPA, XRD and LA-ICP-MS study. *Can Min*
491 50:825-841
- 492 Baksheev IA, Yu P, Zaraisky GP, Chitalin AF, Yapaskurt VO, Nikolaev YN, Tikhomirov PL, Nagornaya EV, Rogacheva L,
493 Gorelikova NV, Kononov OV (2012) Tourmaline as a prospecting guide for the porphyry-style deposits. *Eur J*
494 *Min* 24:957-979
- 495 Beaudoin G, Pitre D (2005) Stable isotope geochemistry of the Archean Val-d'Or (Canada) orogenic gold vein field.
496 *Miner Deposita* 40:59-75
- 497 Belousova EA, Griffin WL, O'Reilly SY, Fisher NI (2002) Apatite as an indicator mineral for mineral exploration: trace-
498 element compositions and their relationship to host rock type. *J Geochem Explor* 76:45-69
- 499 Berryman EJ, Kutzschbach M, Trumbull RB, Meixner A, Van Hinsberg V, Kasemann SA, Franz G (2017) Tourmaline as
500 a petrogenetic indicator in the Pfitsch Formation, western Tauern Window, eastern Alps. *Lithos* 284-285:138-
501 155
- 502 Blewett RS, Squire RJ, Miller JM, Henson PA, Champion DC (2010) Architecture and geodynamic evolution of the St
503 Ives gold field, eastern Yilgarn Craton, Western Australia. *Precam Res* 183:275-291

504 Böhlke JK, Kistler RW (1986) Rb-Sr, K-Ar, and stable isotope evidence for the ages and sources of fluid components of
505 gold-bearing quartz veins in the northern Sierra Nevada foothills metamorphic belt, California. *Econ Geol*
506 81:296-322

507 Chown EH, Hicks J, Phillips GN, Townend R (1982) The disseminated archaean Big Bell gold deposit, Murchison
508 Province, Western Australia: an example of pre-metamorphic hydrothermal alteration. In: Foster RP, Balkema
509 AA (eds) *Gold '82*. Rotterdam,

510 Condie KC (1993) Chemical composition and evolution of the upper continental crust: contrasting results from surface
511 samples and shales. *Chem Geol* 104:1-37

512 Čopjaková R, Skoda R, Vasinova Galiova M, Novak M (2013) Distributions of Y+REE and Sc in tourmaline and their
513 implications for the melt evolution; examples from NYF pegmatites of the Trebic pluton, Moldanubian zone,
514 Czech Republic. *J Geosci* 58:113-131

515 Daoust C, Voicu G, Brisson H, Gauthier M (2011) Geological setting of the Paleoproterozoic Rosebel gold district, Guiana
516 Shield, Suriname. *J South Am Earth Sci* 32:222-245

517 de Iorio M, Ebbels TMD, Stephens DA (2007) Statistical techniques in metabolic profiling. In: Balding DJ, Bishop MJ,
518 Cannings C (eds) *Handbook of statistical genetics*,. 3rd edn. John Wiley & Sons, Chichester, England, pp 347-
519 373

520 De Souza S, Dubé B, McNicoll V, Dupuis C, Mercier-Langevin P, Creaser RA (2014) Fracture-controlled hydrothermal
521 alteration at the Canadian Malartic deposit: Toward a multiphase model for Archean intrusion-related low-
522 grade bulk tonnage gold deposits. GAC-MAC conference

523 De Souza S, Dubé B, McNicoll VJ, Dupuis C, Mercier-Langevin P, Creaser RA, Kjarsgaard IM (2015) Geology,
524 hydrothermal alteration, and genesis of the world-class Canadian Malartic stockwork-disseminated Archean
525 gold deposit, Abitibi, Québec. In: Dube B, Mercier-Langevin P (eds) *Targeted Geoscience Initiative 4:*
526 *contributions to the understanding of precambrian lode gold deposits and implications for exploration*, Open
527 File 7852. pp 113-126

528 Deksis DJ, Koeberl C (2004) Geochemistry, alteration, and genesis of gold mineralization in the Okote area, southern
529 Ethiopia. *Geochem J* 38:307-331

530 Demange M, Pascal ML, Raimbault L, Armand J, Forette MC, Serment R, Touil A (2006) The Salsigne Au-As-Bi-Ag-Cu
531 deposit, France. *Econ Geol* 101:199-234

532 Dietrich RV (1985) *The tourmaline group*. Van Nostrand Reinhold Company, New York

533 Dinel E, Fowler AD, Ayer JA, Still A, Tylee K, Barr E (2008) Lithogeochemical and stratigraphic controls on gold
534 mineralization within the metavolcanic rocks of the Hoyle Pond mine, Timmins, Ontario. *Econ Geol* 103:1341-
535 1363

536 Drivenes K, Larsen RB, Mueller A, Sorensen BE, Wiedenbeck M, Raanes MP (2015) Late magmatic immiscibility during
537 batholith formation; assessment of B isotopes and trace elements in tourmaline from the Land's End Granite,
538 SW England. *Contrib Mineral Petrol* 169:1-27

539 Dubé B, Ravenelle J-F, McNicoll V, Malo M, Nadeau L, Creaser RA, Simoneau J (2011) The world-class Roberto gold
540 deposit, Éléonore property, James Bay area, Superior province, Québec: insights from geology and
541 geochronology. Paper presented at the Geol Assoc Canada-Mineral Assoc Canada-Soc Economic Geologists-
542 SGA Joint Meeting, Ottawa, May 25-27

543 Duchoslav M, Marks MAW, Drost K, McCammon C, Marschall HR, Wenzel T, Markl G (2017) Changes in tourmaline
544 composition during magmatic and hydrothermal processes leading to tin-ore deposition: the Cornubian
545 Batholith, SW England. *Ore Geol Rev* 83:215-234

546 Dutrow BL, Henry DJ (2011) Tourmaline: a geologic DVD. *Elements* 7:301-306

547 Dziggel A, Wulff K, Kolb J, Meyer FM (2009) Processes of high-T fluid-rock interaction during gold mineralization in
548 carbonate-bearing metasediments: the Navachab gold deposit, Namibia. *Miner Deposita* 44:665-687

549 Egozcue JJ, Pawlowsky-Glahn V, Mateu-Figueraz G, Barceló-Vidal C (2003) Isometric logratio transformations for
550 compositional data analysis. *Mathematical Geology* 35:279-300

551 Eilu PK, Mathison CI, Groves DI, Allardyce WJ (1999) Atlas of alteration assemblages, styles and zoning in orogenic
552 lode-gold deposits in a variety of host rock and metamorphic settings, vol 30. University of Western Australia,
553 Geology Department and Extension Service, Perth

554 El Goumi N, De Souza S, Enkin RJ, Dubé B (2015) Petrophysical signature of gold mineralization and alteration
555 assemblages at the Canadian Malartic deposit, Québec. In: Dubé B, Mercier-Langevin P (eds) *Geol Survey*
556 *Canada, Targeted Geoscience Initiative 4: Contributions to the Understanding of Precambrian Lode Gold*
557 *Deposits and Implications for Exploration*, Open File 7852. pp 127-138

558 Eriksson L, Johansson E, Kettaneh-Wold N, Wold S (2001) Multi- and megavariate data analysis basic principles and
559 applications. UMETRICS, Umeå

560 Ertl A, Tillmanns E, Ntaflos T, Francis C, Giester G, Körner W, Hughes JM, Lengauer C, Prem M (2008) Tetrahedrally
561 coordinated boron in Al-rich tourmaline and its relationship to the pressure-temperature conditions of
562 formation. *Eur J Min* 20:881-888

563 Fontaine A, Dubé B, Malo M, McNicoll V, Brisson T (2014) Geology and structural characteristics of the Roberto gold
564 deposit, Eleonore property, Superior Province, Baie James, Québec, Canada. Québec Mines 2014

565 Fontaine A, Dubé B, Malo M, McNicoll V, Brisson T, Doucet D, Goutier J (2015) Geology of the metamorphosed Roberto
566 gold deposit (Éléonore Mine), James Bay region, Quebec: diversity of mineralization styles in a polyphase
567 tectonometamorphic setting. In: Dubé B, Mercier-Langevin P (eds) Targeted Geoscience Initiative 4:
568 Contributions to the Understanding of Precambrian Lode Gold Deposits and Implications for Exploration,
569 Open File 7852. Geol Survey Canada, pp 209-225

570 Gadas P, Novak M, Stanek J, Filip J, Vasinova Galiova M (2012) Compositional evolution of zoned tourmaline crystals
571 from pockets in common pegmatites of the Moldanubian zone, Czech Republic. *Can Min* 50:895-912

572 Galbraith CG, Clarke DB, Trumbull RB, Wiedenbeck M (2009) Assessment of tourmaline compositions as an indicator
573 of emerald mineralization at the Tsa da Glisza prospect, Yukon Territory, Canada. *Econ Geol* 104:713-731

574 Gallagher V, Kennan PS (1992) Tourmaline on the margin of the Leinster granite, southeastern Ireland: petrogenetic
575 implications. *Irish J Earth Sci* 11:131-150

576 Garofalo P, Matthai S, Heinrich C (2002) Three-dimensional geometry, ore distribution and time-integrated mass
577 transfer through the quartz-tourmaline-gold vein network of the Sigma deposit (Abitibi belt, Canada).
578 *Geofluids* 2:217-232

579 Goldfarb RJ, Baker T, Dube B, Groves DI, Hart CJR, Gosselin P (2005) Distribution, character and genesis of gold deposits
580 in metamorphic terranes. In: Hedenquist JW, Thompson JFH, Goldfarb RJ, Richards JP (eds) *Economic Geology*
581 *100th Anniversary Volume*. pp 407-450

582 Goldfarb RJ, Groves DI (2015) Orogenic gold: common or evolving fluid and metal sources through time. *Lithos* 233:2-
583 26

584 Griffin WL, Slack JF, Ramsden AR, Win TT, Ryan CG (1996) Trace elements in tourmalines from massive sulfide
585 deposits and tourmalinites: geochemical controls and exploration applications. *Econ Geol* 91:657-675

586 Grzela D (2017) Tourmaline, scheelite, and magnetite composition from orogenic gold deposits and glacial sediments
587 of the Val-d'Or district (Québec, Canada) Université Laval, Canada

588 Grzela D, Beaudoin G, Bédard É (2019) Tourmaline, scheelite, and magnetite compositions from orogenic gold deposits
589 and glacial sediments of the Val-d'Or district (Québec, Canada): applications to mineral exploration. *J Geochem*
590 *Explor* 206, 106355

591 Hanes R, Huot F, Clevens NR, Goutier J, Beaudoin G, Guilmette C (2017) Orogenic gold veins related to transpressional
592 shear zones along the north-western contact of the La Grande and Opinaca subprovinces, Eeyou Istchee James
593 Bay, Québec, Canada. Proceed 14th SGA Biennial Meeting, Québec, Canada, August 2017

594 Harlaux M (2016) Les systèmes métallogéniques hydrothermaux à tungstène et métaux rares (Nb, Ta, Sn) dans le
595 contexte orogénique finivarisque : exemple du Massif Central français. Université de Lorraine

596 Harlaux M, Kouzmanov K, Gialli S, Laurent O, Marger K, Baumgartner L, Dini A, Chauvet A (2018) Magmatic-
597 hydrothermal transition traced by in situ tourmaline analysis at the San Rafael tin deposit, Peru. *Goldschmidt*
598 2018, Boston

599 Harlaux M, Mercadier J, Marignac C, Villeneuve J, Mouthier B, Cuney M (2019) Origin of the atypical Puy-les-Vingtes W
600 breccia pipe (Massif Central, France) constrained by trace element and boron isotopic composition of
601 tourmaline. *Ore Geol Rev* 114

602 Hazarika P, Mishra B, Pruseth KL (2015) Diverse tourmaline compositions from orogenic gold deposits in the Hutti-
603 Maski greenstone belt, India: implications for sources of ore-forming fluids. *Econ Geol* 110:337-353

604 Hazarika P, Mishra B, Pruseth KL (2016) Scheelite, apatite, calcite and tourmaline compositions from the Late Archean
605 Hutti orogenic gold deposit: implications for analogous two stage ore fluids. *Ore Geol Rev* 72:989-1003

606 Hazarika P, Upadhyay D, Pruseth KL (2017) Episodic tourmaline growth and re-equilibration in mica pegmatite from
607 the Bihar mica belt, India; major and trace element variations under pegmatitic and hydrothermal conditions.
608 *Geol Mag* 154:68-86

609 Hellingwerf RH, Gatedal K, Gallagher V, Baker JH (1994) Tourmaline in the central Swedish ore district. *Miner Deposita*
610 29:189-205

611 Hellmann A, Kolb J, Meyer MF (2005) Physikochemische Bedingungen während amphibolitfazieller hydrothermaler
612 Goldmineralisation-Hira Buddinni, Indien. *Eur J Min* 17:54

613 Hellmann A (2009) The genesis of the gold deposit Hira Buddini, South India (in German). Rheinisch -Westfälischen
614 Technischen Hochschule, Aachen

615 Henry DJ, Guidotti CV (1985) Tourmaline as a petrogenetic indicator mineral: an example from the staurolite-grade
616 metapelites of NW Maine. *Am Mineral* 70:1-15

617 Henry DJ, Dutrow BL (1996) Metamorphic tourmaline and its petrologic applications. In: Grew ES, Anovitz LM (eds)
618 Boron: mineralogy, petrology and geochemistry Review in Mineral 33.

619 Henry DJ, Sun H, Slack JF, Dutrow BL (2008) Tourmaline in meta-evaporites and highly magnesian rocks; perspectives
620 from Namibian tourmalinites. Eur J Min 20:889-904

621 Henry DJ, Novak M, Hawthorne FC, Ertl A, Dutrow BL, Uher P, Pezzotta F (2011) Nomenclature of the tourmaline-
622 supergroup minerals. Am Mineral 96:895-913

623 Hong W, Cooke DR, Zhang L, Fox N, Thompson J (2017) Tourmaline-rich features in the Heemskirk and Pieman Heads
624 granites from western Tasmania, Australia: characteristics, origins, and implications for tin mineralization.
625 Am Mineral 102:876-899

626 Hoskin PWO, Schaltegger U (2003) The composition of zircon and igneous and metamorphic petrogenesis. In: Hanchar
627 JM, Hoskin PWO (eds) Zircon Rev in Mineral and Geochem, vol 53. p 550

628 Hron K, Templ M, Filzmoser P (2010) Imputation of missing values for compositional data using classical and robust
629 methods. Computational Statistics and Data Analysis 54:3095-3107

630 IAMGold (2009) Updated feasibility study - Essakane Gold project Burkina Faso

631 Iveson AA, Webster JD, Rowe MC, Neill OK (2016) Magmatic-hydrothermal fluids and volatile metals in the Spirit Lake
632 pluton and Margaret Cu-Mo porphyry system, SW Washington, USA. Contr Mineral Petrol 171:20

633 Jiang S-Y, Han F, Shen J, Palmer MR (1999) Chemical and Rb-Sr, Sm-Nd isotopic systematics of tourmaline from the
634 Dachang Sn-polymetallic ore deposit, Guangxi Province, P.R. China. Chem Geol 157:49-67

635 Jiang S-Y, Palmer MR, Yeats CJ (2002) Chemical and boron isotopic compositions of tourmaline from the Archean Big
636 Bell and Mount Gibson gold deposits, Murchison Province, Yilgarn Craton, Western Australia. Chem Geol
637 188:229-247

638 Jiang S-Y, Yu J-M, Lu J-J (2004) Trace and rare-earth element geochemistry in tourmaline and cassiterite from the
639 Yunlong tin deposit, Yunnan, China: implication for migmatitic-hydrothermal fluid evolution and ore genesis.
640 Chem Geol 209:193-213

641 Jolliff BL, Papike JJ, Laul JC (1987) Mineral recorders of pegmatite internal evolution: REE contents of tourmaline from
642 the Bob Ingersoll pegmatite, South Dakota. Geochim Cosmochim Acta 51:2225-2232

643 Joyce NJ (2016) Alteration mineralogy and pathfinder element inventory in the footprint of the McArthur River
644 unconformity-related uranium deposit, Canada. Queen's University, Kingston, Ontario, Canada, Depart
645 Geological Sciences and Geological Engineering

646 Kalliomäki H, Wagner T, Fusswinkel T, Sakellaris G (2017) Major and trace element geochemistry of tourmalines from
647 Archean orogenic gold deposits: proxies for the origin of gold mineralizing fluids? *Ore Geol Rev* 91:906-927

648 Keller P, Roda Robles E, Pesquera Pérez A, Fontan F (1999) Chemistry, paragenesis and significance of tourmaline in
649 pegmatites of the southern tin belt, central Namibia. *Chem Geol* 158:203-225

650 Kempe U, Belyatsky B, Krymsky R, Kremenetsky AA, Ivanov PA (2001) Sm-Nd and Sr isotope systematics of scheelite
651 from the giant Au(-W) deposit Muruntau (Uzbekistan): implications for the age and sources of Au
652 mineralization. *Miner Deposita* 36:379-392

653 Kerrich R (1989) Geochemical evidence on the sources of fluids and solutes for shear zone hosted mesothermal Au
654 deposits. In: Bursnell JT (ed) *Mineralization and shear zones*, Geol Assoc Canada Short Course 6. pp 129-197

655 Kerrich R (1993) Perspectives on Genetic Models for Lode Gold Deposits. *Miner Deposita* 28:362-365

656 King RW, Goode ADT, Smyth EL, Birch WD, Bosma LI (1988) Geochemical characteristics of tourmaline from Superior
657 Province Archaean lode gold deposits; implications for source regions and processes. *Geol Soc Australia*
658 23:445-447

659 King RW, Kerrich R (1989) Chromian dravite associated with ultramafic-rock-hosted Archean lode gold deposits,
660 Timmins-Porcupine district, Ontario. *Can Min* 27:419-426

661 Kisters AFM (2005) Controls of gold-quartz vein formation during regional folding in amphibolite-facies, marble-
662 dominated metasediments of the Navachab gold mine in the Pan-African Damara Belt, Namibia. *South Afr J*
663 *Geol* 108:365-380

664 Klemme S, Marschall HR, Jacob DE, Prowatke S, Ludwig T (2011) Trace-element partitioning and boron isotope
665 fractionation between white mica and tourmaline. *Can Min* 49:165-176

666 Kolb J, Rogers A, Meyer FM (2005) Relative timing of deformation and two-stage gold mineralization at the Hutti mine,
667 Dharwar Craton, India. *Miner Deposita* 40:156-174

668 Kositcin N, McNaughton NJ, Griffin BJ, Fletcher IR, Groves DI, Rasmussen B (2003) Textural and geochemical
669 discrimination between xenotime of different origin in the Archaean Witwatersrand Basin, South Africa.
670 *Geochim Cosmochim Acta* 67:709-731

671 Koval PV, Zorina LD, Kitajev NA, Spiridonov AM, Ariunbileg S (1991) The use of tourmaline in geochemical prospecting
672 for gold and copper mineralization. *J Geochem Explor* 40:349-360

673 Krienitz M, Trumbull R, Hellmann A, Kolb J, Meyer F, Wiedenbeck M (2008) Hydrothermal gold mineralization at the
674 Hira Buddini gold mine, India: constraints on fluid evolution and fluid sources from boron isotopic
675 compositions of tourmaline. *Miner Deposita* 43:421-434

676 Krosse S (1995) Hochdrucksynthese, stabilität und eigenschaften der borsilikate dravit und kornerupin, sowie
677 darstellung und stabilitätsverhalten eines neuen Mg-Al-borates. Ruhr-Universität Bochum

678 Launay G, Sizaret S, Guillou-Frottier L, Gloaguen E, Pinto F (2018) Deciphering fluid flow at the magmatic-
679 hydrothermal transition: a case study from the world-class Panasqueira W-Sn-(Cu) ore deposit (Portugal).
680 *Earth Planet Sci Lett* 499:1-12

681 Leach DL, Sangster DF, Kelley KD, Large RR, Garven G, Allen CR, Gutzmer J, Walters S (2005) Sediment-hosted lead-zinc
682 deposits: A global perspective *Economic Geology* 100th Anniversary Volume. pp 561-607

683 Longerich HP, Jackson SE, Günther D (1996) Laser ablation inductively coupled plasma mass spectrometric transient
684 signal data acquisition and analyte concentration calculation. *Journal of Analytical Atomic Spectrometry*, 11,
685 899-904. *J Analytical Atomic Spectrometry* 11:899-904

686 Lottermoser BG, Plimer IR (1987) Chemical variation in tourmalines Umberatana, South Australia. *Neues Jahrbuch*
687 *Min Monatshefte* 7:314-327

688 Makvandi S, Ghasemzadeh-Barvarz M, Beaudoin G, Grunsky EC, McClenaghan MB, Duchesne C (2016a) Principal
689 component analysis of magnetite composition from volcanogenic massive sulfide deposits: case studies from
690 the Izok Lake (Nunavut, Canada) and Halfmile Lake (New Brunswick, Canada) deposits. *Ore Geol Rev* 72:60-
691 85

692 Makvandi S, Ghasemzadeh-Barvarz M, Beaudoin G, Grunsky EC, McClenaghan MB, Duchesne C, Boutroy E (2016b)
693 Partial least squares-discriminant analysis of trace element compositions of magnetite from various VMS
694 deposit subtypes: application to mineral exploration. 78:388-408

695 Manégliá N (2017) Indicator minerals composition in the Meliadine district and glacial sediments (Nunavut, Canada).
696 Université Laval, Canada

697 Manégliá N, Beaudoin G, Simard M (2018) Indicator minerals of the Meliadine orogenic gold deposits, Nunavut
698 (Canada), and application to till surveys. *Geochem: Explor, Environ, Anal* 18:241-251

699 Mao M, Rukhlov AS, Rowins SM, Spence J, Coogan LA (2016) Apatite trace element compositions; a robust new tool for
700 mineral exploration. *Econ Geol* 111:1187-1222

701 Marcoux É, Lescuyer J-L (1994) Les minerais sulfo-arseniés aurifères de Salsigne, Aude, France: évolution
702 paragenétique d'une minéralisation ardi-hercynienne syntectonique en contexte sédimentaire. *Canad Mineral*
703 32:159-177

704 Marks MAW, Marschall HR, Schuehle P, Guth A, Wenzel T, Jacob DE, Barth M, Markl G (2013) Trace element systematics
705 of tourmaline in pegmatitic and hydrothermal systems from the Variscan Schwarzwald (Germany): the
706 importance of major element composition, sector zoning, and fluid or melt composition. *Chem Geol* 344:73-
707 90

708 Marschall H, Jiang S (2011) Tourmaline isotopes: no element left behind. *Elements* 7:313-319

709 Martin R (2012) Syenite-hosted gold mineralization and hydrothermal alteration at the Young-Davidson deposit,
710 Matachewan, Ontario. University of Waterloo, Earth Science Dept, Canada

711 McCuaig C, T., Kerrich R (1998) P-T-t-deformation-fluid characteristics of lode gold deposits: evidence from alteration
712 systematics. *Ore Geol Rev* 12:381-453

713 McDonough WF, Sun Ss (1995) The composition of the Earth. *Chem Geol* 120:223-253

714 McGoldrick KL, Squire RJ, Cas RAF, Briggs M, Tunjic J, Allen CM, Campbell IH, Hayman PC (2013) The largest Au
715 deposits in the St Ives gold field (Yilgarn Craton, Western Australia) may be located in a major Neoproterozoic
716 volcano-sedimentary depo-centre. *Miner Deposita* 48:861-881

717 Migdisov A, Williams-Jones AE, Brugger J, Caporuscio FA (2016) Hydrothermal transport, deposition, and fractionation
718 of the REE; experimental data and thermodynamic calculations. *Chem Geol* 439:13-42

719 Miller LJ, Goldfarb RJ, Snee LW, Gent CA, Kirkham RA (1995) Structural geology, age, and mechanisms of gold vein
720 formation at the Kensington and Jualin deposits, Berners Bay district, southeast Alaska. *Econ Geol* 90:343-368

721 Moritz RP, Crocket JH (1990) Mechanics of formation of the gold-bearing quartz-fuchsite vein at the Dome mine,
722 Timmins area, Ontario. Canada *J Earth Sci* 27:1609-1620

723 Mueller AG, De Laeter JR, Groves DI (1991) Strontium isotope systematics of hydrothermal minerals from epigenetic
724 Archean gold deposits in the Yilgarn block, Western Australia. *Econ Geol* 86:780-809

725 Mueller AG, Campbell IH, Schiotte L, Sevigny JH, Layer PW (1996) Constraints on the age of granitoid emplacement,
726 metamorphism, gold mineralization, and subsequent cooling of the Archean greenstone terrane at Big Bell,
727 Western Australia. *Econ Geol* 91:896-915

728 Neumayr P, Walshe J, Hagemann S, Petersen K, Roache A, Frikken P, Horn L, Halley S (2008) Oxidized and reduced
729 mineral assemblages in greenstone belt rocks of the St. Ives gold camp, Western Australia: vectors to high
730 grade ore bodies in Archaean gold deposits? *Miner Deposita* 43:363-371

731 Nörtemann MF-J, Mücke A, Weber K, Meinert LD (2000) Mineralogy of the Navachab skarn deposit, Namibia: an
732 unusual Au-bearing skarn in high-grade metamorphic rocks. *Commun Geol Survey Namibia* 12:169-177

733 Orlando A, Ruggieri G, Chiarantini L, Montegrossi G, Rimondi V (2017) Experimental Investigation of Biotite-Rich
734 Schist Reacting with B-Bearing Fluids at Upper Crustal Conditions and Correlated Tourmaline Formation.
735 *Minerals* 7:155

736 Ota T, Kobayashi K, Katsura T, Nakamura E (2008) Tourmaline breakdown in a pelitic system: implications for boron
737 cycling through subduction zones. *Contrib Mineral Petrol* 155:19-32

738 Otto A (2007) Tektono-metamorphe kontrolle der archaischen goldmineralisation in der New Consort gold mine,
739 Barberton Grünsteingürtel, Südafrika. Rheinisch - Westfälischen Technischen Hochschule, Germany

740 Otto A, Dziggel A, Kisters AFM, Meyer FM (2007) The New Consort gold mine, Barberton greenstone belt, South Africa;
741 orogenic gold mineralization in a condensed metamorphic profile. *Miner Deposita* 42:715-735

742 Pesquera A, Torres-Ruiz J, Gil-Crespo PP, Jiang SY (2005) Petrographic, chemical and B-isotopic insights into the origin
743 of tourmaline-rich rocks and boron recycling in the Martinamor antiform (central Iberian zone, Salamanca,
744 Spain). *J Petrol* 46:1013-1044

745 Phillips GN, Nooy DD (1988) High-grade metamorphic processes which influence Archaean gold deposits, with
746 particular reference to Big Bell, Australia. *J Meta Geol* 6:95-114

747 Poulsen KH, Robert F, Dubé B (2000) Geological classification of Canadian gold deposits. *Geol Survey Canada Bulletin*
748 540, Ottawa

749 Proudlove DC, Hutchinson RH, Rogers DS (1988) Multiphase mineralization in concordant and discordant gold veins,
750 Dome mine, South Porcupine, Ontario, Canada. In Keays RR, Ramsay, WRH, Groves, DI (eds) *The geology of*
751 *gold deposits: the perspective in 1988*. *Econ Geol Monogr* 6:112-123

752 Raith JG, Riemer NS, Meisel T (2004) Boron metasomatism and behaviour of rare earth elements during formation of
753 tourmaline rocks in the eastern Arunta Inlier, central Australia. *Contrib Mineral Petrol* 147:91-109

754 Ravenelle J-F, Dubé B, Malo M, McNicoll V, Nadeau L, Simoneau J (2010) Insights on the geology of the world-class
755 Roberto gold deposit, Éléonore property, James Bay area, Québec, *Geol Survey Canada, Current Research*
756 2010-1

757 Ravenelle J-F (2013) Amphibolite facies gold mineralization: an example from the Roberto deposit, Éléonore property,
758 James Bay, Québec. Université Québec Institut National de la Recherche Scientifique Centre Eau Terre
759 Environnement

760 Reynolds DG (1965) Geology and mineralization of the Salsigne gold mine, France. *Econ Geol* 60:772-791

761 Ridley J (2013) *Ore deposit geology*. Cambridge University Press, Cambridge, UK

762 Roberts S, Palmer MR, Waller L (2006) Sm-Nd and REE characteristics of tourmaline and scheelite from the Bjorkdal
763 gold deposit, northern Sweden: evidence of an intrusion-related gold deposit? *Econ Geol* 101:1415-1425

764 Roda-Robles E, Pesquera A, Gil PP, Torres-Ruiz J, Fontan F (2004) Tourmaline from the rare-element Pinilla pegmatite,
765 (central Iberian zone, Zamora, Spain); chemical variation and implications for pegmatitic evolution. *Miner
766 Petrol* 81:249-263

767 Roda-Robles E, Pesquera A, Gil-Crespo PP, Torres-Ruiz J (2011) Occurrence, paragenesis and compositional evolution
768 of tourmaline from the Tormes Dome area, central Iberian zone, Spain. *Can Min* 49:207-224

769 Roda-Robles E, Pesquera A, Gil-Crespo P, Torres-Ruiz J (2012) From granite to highly evolved pegmatite; a case study
770 of the Pinilla de Fermoselle granite-pegmatite system (Zamora, Spain). *Lithos* 153:192-207

771 Roda-Robles E, Simmons W, Pesquera A, Gil-Crespo PP, Nizamoff J, Torres-Ruiz J (2015) Tourmaline as a petrogenetic
772 monitor of the origin and evolution of the Berry-Havey pegmatite (Maine, U.S.A.). *Am Mineral* 100:95-109

773 Roda E, Pesquera A, Velasco F (1995) Tourmaline in granitic pegmatites and their country rocks, Fregeneda area,
774 Salamanca, Spain. *Can Min* 33:835-848

775 Rubatto D (2002) Zircon trace element geochemistry: partitioning with garnet and the link between U-Pb ages and
776 metamorphism. *Chem Geol* 184:123-138

777 Rumsey D, Safari aORMC (2011) *Statistics for dummies, 2nd Ed, for dummies*

778 Schneider DA, Bachtel J, Schmitt AK (2012) Zircon alteration in wall rock of Pamour and Hoyle Pond Au deposits,
779 Abitibi greenstone belt: constraints on timescales of fluid flow from depth-profiling techniques. *Econ Geol*
780 107:1043-1072

781 Sciuba M, Beaudoin G, Grzela D, Makvandi S (2020) Trace element composition of scheelite in orogenic gold deposits.
782 *Miner Deposita*

783 Selway JB, Novak M, Černý P, Hawthorne FC (1999) Compositional evolution of tourmaline in lepidolite-subtype
784 pegmatites. *Eur J Min* 11:569-584

785 Selway JB, Černý P, Hawthorne FC, Novak M (2000) The Tanco pegmatite at Bernic Lake, Manitoba. *Can Min* 38:877-
786 891

787 Slack JF, Coad PR (1989) Multiple hydrothermal and metamorphic events in the Kidd Creek volcanogenic massive
788 sulphide deposit, Timmins, Ontario: evidence from tourmalines and chlorites. *Canada J Earth Sci* 26:694-715

789 Slack JF, Palmer MR, Stevens BPJ, Barnes RG (1993) Origin and significance of tourmaline-rich rocks in the Broken Hill
790 district, Australia. *Econ Geol* 88:505-541

791 Slack JF (1996) Tourmaline associations with hydrothermal ore deposits. In: Grew ES, Anovitz LM (eds) *Boron:*
792 *mineralogy, petrology and geochemistry*, *Rev Mineral* 33, pp 559-643

793 Slack JF, Ramsden AR, Griffin WL, Win TT, French DH, Ryan CG (1999) Trace elements in tourmaline from the Kidd
794 Creek massive sulfide deposit and vicinity, Timmins, Ontario: a proton microprobe Study. In: Hannington MD,
795 Barrie T (eds) *The giant Kidd Creek volcanogenic massive sulfide deposit, Western Abitibi subprovince,*
796 *Canada. Econ Geol Monog* 10, pp 415-430

797 Slack JF (2002) Tourmaline associations with hydrothermal ore deposits. In: Grew ES, Anovitz LM (eds) *Boron:*
798 *Mineralogy, Petrology and Geochemistry*, vol 33. *Reviews in Mineralog*

799 Slack JF, Trumbull R (2011) Tourmaline as a recorder of ore-forming processes. *Elements* 7:321-326

800 Smith EJ, Kesler SE, Van Hees EHP (1987) Relationship of fluid inclusion geochemistry to wall-rock alteration and
801 lithogeochemical zonation at the Hollinger-McIntyre gold deposit, Porcupine district, Canada. *J Geochem*
802 *Explor* 29:434

803 Smith TJ, Cloke PL, Kesler SE (1984) Geochemistry of fluid inclusions from the McIntyre-Hollinger gold deposit,
804 Timmins, Ontario, Canada. *Econ Geol* 79:1265-1285

805 Steenkamp HM, Guilmette C, Wodicka N (2016) New insights into regional metamorphism of the Tehery-Wager area,
806 southwestern Rae craton, Nunavut, Canada. *Geol Assoc Canada-Min Assoc Canada, Pgm Abs*

807 Sun SS, McDonough WF (1989) Chemical and isotopic systematics of oceanic basalts: implications for mantle
808 composition and processes. In: Saunders AD, Norry MJ (eds) *Magmatism in the Ocean Basins*, Special
809 publication 42. Geological Society, London, pp 313-345

810 Tahmasbi Z, Zal F, Khalaji AA (2017) Geochemistry and formation of tourmaline nodules in Mashhad leucogranite,
811 Iran. *Geosci J* 21:341-353

812 Taylor BE, Slack JF (1984) Tourmalines from Appalachian-Caledonian massive sulfide deposits: textural, chemical, and
813 isotopic relationships. *Econ Geol* 79:1703-1726

814 Taylor RD, Goldfarb RJ, Monecke T, Fletcher IR, Cosca MA, Kelly NM (2015) Application of U-Th-Pb phosphate
815 geochronology to young orogenic gold deposits; new age constraints on the formation of the Grass Valley gold
816 district, Sierra Nevada foothills province, California. *Econ Geol* 110:1313-1337

817 Thió-Henestrosa S, Martín-Fernández JA (2005) Dealing with compositional data: the freeware CoDaPack.
818 *Mathematical Geology* 37:773-793

819 Van Hinsberg VJ, Schumacher JC (2007) Using estimated thermodynamic properties to model accessory phases: the
820 case of tourmaline. *J Meta Geol* 25:769-779

821 Van Hinsberg VJ, Schumacher JC (2009) The geothermobarometric potential of tourmaline, based on experimental and
822 natural data. *Am Mineral* 94:761-770

823 Van Hinsberg VJ (2011) Preliminary experimental data on trace-element partitioning between tourmaline and silicate
824 melt. *Can Min* 49:153-163

825 Van Hinsberg VJ, Henry DJ, Marschall HR, Martin RF (2011) Tourmaline: an ideal indicator of its host environment.
826 *Can Min* 49:1-16

827 Van Hinsberg VJ, Schumacher JC (2011) Tourmaline as a petrogenetic indicator mineral in the Haut-Allier
828 metamorphic suite, Massif Central, France. *Can Min* 49:177-194

829 Vielreicher NM, Groves DI, Fletcher IR, McNaughton NJ, Rasmussen B (2003) Hydrothermal monazite and xenotime
830 geochronology; a new direction for precise dating of orogenic gold mineralization. *SEG Newsletter* 53:1, 10-
831 16

832 Wang Z, Chen B, Yan X (2018) Geochemistry and boron isotopic compositions of tourmaline from the Paleoproterozoic
833 amphibolites, NE China: Implications for the origin of borate deposit. *Precam Res* 326:258-271

834 Whitten E (1995) Open and closed compositional data in petrology. *Mathematical Geology* 27:789-806

835 Wilkins C (1993) A post-deformational, post-peak metamorphic timing for mineralization at the Archaean Big Bell
836 gold deposit, Western Australia. *Ore Geol Rev* 7:439-483

837 Williamson BJ, Spratt J, Adams JT, Tindle AG, Stanley CJ (2000) Geochemical constraints from zoned hydrothermal
838 tourmalines on fluid evolution and Sn mineralization: an example from fault breccias at Roche, SW England. *J*
839 *Petrol* 41:1439-1453

840 Wood PC, Burrows DR, Spooner ETC (1986) Au-quartz vein and intrusion-hosted Cu-Au-Ag-Mo mineralization,
841 Hollinger-McIntyre mines, Timmins, Ontario; geological characteristics, structural examination, igneous and

842 hydrothermal alteration geochemistry, and light stable isotope (hydrogen and oxygen) geochemistry. Ontario
843 Geol Survey Miscellaneous Paper 130:115-137

844 Wulff K (2008) Petrography, geochemistry and stable isotope characteristics of the Navachab gold deposit, Namibia.
845 Doctoral, Rheinisch Westfälischen Technischen Hochschule Aachen University

846 Yang S, Jiang S, Palmer MR (2015a) Chemical and boron isotopic compositions of tourmaline from the Nyalam
847 leucogranites, south Tibetan Himalaya; implication for their formation from B-rich melt to hydrothermal
848 fluids. *Chem Geol* 419:102-113

849 Yang S, Jiang S, Zhao K, Dai B, Yang T (2015b) Tourmaline as a recorder of magmatic-hydrothermal evolution: an in
850 situ major and trace element analysis of tourmaline from the Qitianling Batholith, South China. *Contrib
851 Mineral Petrol* 170:1-21

852 Yavuz F, Iskenderoglu A, Jiang S (1999) Tourmaline compositions from the Salikvan porphyry Cu-Mo deposit and
853 vicinity, northeastern Turkey. *Can Min* 37:1007-1023

854 Yavuz F, Jiang S-Y, Karakaya N, Karakaya MÇ, Yavuz R (2011) Trace-element, rare-earth element and boron isotopic
855 compositions of tourmaline from a vein-type Pb-Zn-Cu±U deposit, NE Turkey. *Int Geol Rev* 53:1-24

856 Zack T, Kronz A, Foley SF, Rivers T (2002) Trace element abundances in rutiles from eclogites and associated garnet
857 mica schists. *Chem Geol* 184:97-122

858 Zhang J, Lin S, Linnen R, Martin R (2014) Structural setting of the Young-Davidson syenite-hosted gold deposit in the
859 western Cadillac-Larder Lake deformation zone, Abitibi greenstone belt, Superior Province, Ontario. *Precam
860 Res* 248:39-59

861

862 **Figures captions**

863 Fig. 1. Photomicrographs showing tourmaline textures and mineral associations in orogenic gold deposits; all plane
864 polarized light except f (left side plane polarized; right side reflected light) (a) disseminated euhedral greenish
865 tourmaline (Royal Hill, Rosebel, Suriname), (b) disseminated euhedral tourmaline with light blue core and subtle
866 orange rim (Hoyle Pond, Canada), (c) aggregate of subhedral orange tourmaline (Roberto, Canada), (d) aggregate of
867 subhedral tourmaline with bluish grey core and greenish brown rim (Canadian Malartic, Canada), (e) disseminated
868 subhedral tourmaline with greyish core and brownish rim associated with sulfides (New Consort, South Africa), (f)
869 aggregate of subhedral orange to brown tourmaline associated with gold (Essakane, Burkina Faso) on the left in
870 transmitted light and on the right in reflected light. Abbreviations: Au: native gold, Carb: carbonate, Chl: chlorite, Po:
871 pyrrhotite, Py: pyrite, Qz: quartz, Tur: tourmaline.

872 Fig. 2. Back-scattered electron images of zoned tourmaline in orogenic gold deposits, (a) complex sector zoning
873 (Essakane, Burkina Faso), (b) oscillatory zoning coupled with sector zoning (Salsigne, France), (c) oscillatory and
874 sector zoning (TR98-111, James Bay, Canada), (d) diffuse zoning and inclusions (Nevada, USA), (e) narrow rim with
875 large core (New Consort, South Africa), (f) irregular zoning (Big Bell, Australia). Abbreviations: Bt: biotite, Fsp:
876 feldspar, Py: pyrite, Qz: quartz, Ser: sericite, Tur: tourmaline.

877 Fig. 3. (a) Major, minor and (b) trace elements concentrations sorted by median tourmaline composition for orogenic
878 gold deposits, measured by EPMA and LA-ICP-MS. See ESM 1 Tables T2 and T3 for EPMA and LA-ICP-MS data,
879 respectively.

880 Fig. 4. (a) Back-scattered electron images of zoned tourmaline in pyrite and EPMA maps (512 x 512 pixels) (b) Ti (c)
881 Fe, (d) Ca, (e) Mg, (f) V. Sample TR98-111 showing from James Bay, Canada.

882 Fig. 5. Composition of tourmaline from orogenic gold deposits and other deposit types and settings (a) X-Vacancy-Ca-
883 (Na+K) ternary diagram (b) Mg/(Fe+Mg) vs Vac/(Na+K+Vac) diagram and (c) Mg/(Fe+Mg) vs Ca/(Ca+Na) diagram.
884 Diagrams adapted from Henry et al. (2011).

885 Fig. 6. Binary plots of LA-ICP-MS trace element data for tourmaline from orogenic gold deposits (a) La vs Zr, (b) Yb vs
886 Zr, (c) Σ REE vs Zr, (d) Zr vs Hf, (e) Fe vs Sn, (f) Σ REE vs Ti, (g) Eu anomaly vs Y, (h) Ni vs Co and, (i) Σ REE vs Ga. Data
887 from literature: Lottermoser and Plimer 1987; Slack and Coad 1989; Gallagher and Kennan 1992; Jiang et al. (2002);
888 Deksisssa and Koeberl (2004); Roberts et al. (2006); Hazarika et al. (2015); Hazarika et al. (2016); Grzela (2017);
889 Kalliomäki et al. (2017); Manégliá (2017).

890 Fig. 7. Rare earth element patterns with mean (thick line) for tourmaline from orogenic gold deposits. Data are
891 normalized to chondrite from McDonough and Sun (1995). The individual deposit patterns are in ESM 2 Fig. S9.

892 Fig. 8. Binary plots of Eu anomaly vs $(La/Sm)_{CN}$ (LA-ICP-MS data) for tourmaline from (a) various deposit types and
893 (b) orogenic gold deposits only. “m+” refers to a positive slope and “m-” refers to a negative slope. Data from literature:
894 Lottermoser and Plimer 1987; Slack and Coad 1989; Gallagher and Kennan 1992; Jiang et al. (2002); Deksisssa and
895 Koeberl (2004); Roberts et al. (2006); Hazarika et al. (2015); Hazarika et al. (2016); Grzela (2017); Kalliomäki et al.
896 (2017); Manégliá (2017).

897 Fig. 9. PLS-DA of LA-ICP-MS data for tourmaline in orogenic gold deposits hosted in country rocks with diverse
898 compositions. (a) qw^*_1 - qw^*_2 loadings show correlations among chemical elements and country rock classes, (b) t_1 - t_2
899 scores shows distribution of tourmaline data from within space defined by qw^*_1 - qw^*_2 , and, (c) VIP values show
900 importance of compositional variables in classification of different country rock classes. Data for orogenic gold
901 deposits include results from Grzela (2017) and Manégliá (2017).

902 Fig. 10. PLS-DA of LA-ICP-MS data for tourmaline from orogenic gold deposits hosted in country rocks with diverse
903 compositions and in various metamorphic grades. (a) qw^*_1 - qw^*_2 loadings show correlations among chemical elements
904 and classes defined by composition and metamorphic facies of country rocks, (b) t_1 - t_2 scores shows distribution of
905 tourmaline data within the space defined by qw^*_1 - qw^*_2 , and (c) VIP values show importance of compositional
906 variables in classification defined by composition and metamorphic facies of country rocks. Data for orogenic gold
907 deposits include results of Grzela (2017) and Manégliá (2017).

908 Fig. 11. Binary plots of trace element data for tourmaline from various deposit types and geological settings (a) Sr vs
909 V, (b) Nb vs V, (c) Li vs Sn, (d) Ta vs Be, (e) Sr/Li vs V/Sn, (f) Sr/Sn vs V/Nb, (g) Ta vs Ni, (h) Nb vs Ga and, (i) Sr/Sn vs
910 Ba. Data for orogenic gold deposits from Jiang et al. (2002); Deksissa and Koeberl (2004); Roberts et al. (2006);
911 Hazarika et al. (2015); Hazarika et al. (2016); Grzela (2017); Kalliomäki et al. (2017); Manégli (2017).

912 Fig. 12. PLS-DA from LA-ICP-MS data for tourmaline from various deposit types and rocks using Li, Sc, V, Co, Zn, Sr, Sn,
913 and Pb (a) qw^*_1 - qw^*_2 loadings show correlations among elemental variables and classes defined by deposit types and
914 geological environments, (b) t_1 - t_2 scores shows distribution of tourmaline data within space defined by qw^*_1 - qw^*_2 ,
915 and (c) VIP values show importance of compositional variables in classifications defined by deposit types and
916 geological environments.

917 **Table captions**

918 Table 1. Geological settings of studied gold deposits.

919 Table 2. Characteristics of tourmaline for each gold deposit.

920 Table 3. Median trace element compositions in tourmaline from orogenic gold deposits divided by the metamorphic
921 facies of the country rocks.

922 **Electronic Supplementary Material**

923 ESM 1. Tables

924 T1. Analytical conditions for trace element analyses in tourmaline by LA-ICP-MS.

925 T2. EPMA elements composition in tourmaline from orogenic gold deposits and other localities.

926 T3. LA-ICP-MS trace elements composition in tourmaline from orogenic gold deposits and other localities.

927 T4. Correlation matrix among HFSE, LILE and compatible elements for tourmaline from orogenic gold deposits.
928 Coefficients greater than 0.60 are in bold, coefficients between 0.40 and 0.60 are in italics.

929

930 ESM 2. Figures

931 S1. Comparison between LA-ICP-MS and EPMA analyses for (a) Na, (b) Ca, (c) K, (d) Fe, (e) Al, (f) Mg, (g) Mn, (h) Ni, (i)
932 Zn, (j) Ti, (k) V and (l) Sc. Red line – 1:1 slope.

933 S2. Partial Least Square Discriminant Analysis with EPMA major elements for tourmaline in orogenic gold deposits
934 hosted in various country rock compositions. (a) qw^*_1 - qw^*_2 loadings, (b) t_1 - t_2 scores, (c) VIP. Data from the literature:
935 Grzela (2017) and Manégliá (2017).

936 S3. Binary plot of Mn vs Ti with color variation under non polarized light of EPMA data in tourmaline from orogenic
937 gold deposits.

938 S4. LA-ICP-MS trace element binary plots for tourmaline from orogenic gold deposits (a) Σ REE vs Sn, (b) Σ REE vs Hf,
939 (c) Σ REE vs Zr, (d) Σ REE vs Nb, (e) Σ REE vs Th, (f) Σ REE vs U and, (g) Σ REE vs Y. Data from the literature: Jiang et al.
940 (2002); Deksissa and Koeberl (2004); Roberts et al. (2006); Hazarika et al. (2015); Hazarika et al. (2016); Grzela
941 (2017), Kalliomäki et al. (2017) and Manégliá (2017).

942 S5. LA-ICP-MS trace element binary plots for tourmaline from orogenic gold deposits (a) Y vs Zr, (b) Ta vs Nb, (c) Th
943 vs U, (d) Ga vs Sn, (e) Sc vs V and and, (f) Cr vs Mg. Data from the literature: Jiang et al. (2002); Deksissa and Koeberl
944 (2004); Roberts et al. (2006); Hazarika et al. (2015); Hazarika et al. (2016); Grzela (2017), Kalliomäki et al. (2017) and
945 Manégliá (2017).

946 S6. REE binary plots for tourmaline in orogenic gold deposits (a) $(La/Yb)_{CN}$ vs Σ REE, (b) $(La/Sm)_{CN}$ vs Sm_{CN} , (c)
947 $(Gd/Yb)_{CN}$ vs Yb_{CN} , (d) $(La/Sm)_{CN}$ vs Σ LREE and and, (e) $(Gd/Yb)_{CN}$ vs Σ HREE. “m+” refers to a positive slope and “m-”
948 refers to a negative slope. Data from the literature: King et al. (1988), Jiang et al. (2002), Deksissa and Koeberl (2004),
949 Roberts et al. (2006), Hazarika et al. (2015), Hazarika et al. (2016), Grzela (2017), Manégliá (2017) and Kalliomäki et
950 al. (2017).

951 S7. Major and minor element variation with zoning in tourmaline from orogenic gold deposits from LA-ICP-MS maps;
952 (a) microphotograph in plane polarized light of tourmaline from Rosebel (Suriname); (b) Fe; (c) Mg; (d) Ca; (e) V; (f)
953 Ti; (g) microphotograph in plane polarized light of tourmaline from Excelsior (USA); (h) Fe; (i) Mg; (j) Ca; (k) V; (l) Ti;
954 (m) microphotograph in plane polarized light of tourmaline from Hoyle Pond (Canada); (n) Fe; (o) Mg; (p) Ca; (q) V
955 and (r) Ti. Abbreviations: Carb: carbonate, Chl: chlorite, Qz: quartz, Tur: tourmaline.

956 S8. Partial Least Square Discriminant Analysis of LA-ICP-MS data for tourmaline from orogenic gold deposits hosted
957 in various country rock compositions and formed at various ages. (a) qw^*_1 - qw^*_2 loadings, (b) t_1 - t_2 scores and (c) VIP.
958 Data from the literature : Grzela (2017) and Manégliá (2017).

959 S9. Rare earth elements patterns from LA-ICP-MS data in tourmaline core from orogenic gold deposits; (a) Hollinger
960 (Canada); (b) Hoyle Pond (Canada); (c) Young Davidson (Canada); (d) Canadian Malartic (Canada); (e) Roberto
961 (Canada); (f) James Bay (Canada); (g) Excelsior (USA); (h) Rosebel (Suriname); (i) Essakane (Burkina Faso); (j) New
962 Consort (South Africa); (k) Hira Buddini (India); (l) Uti (India); (m) Big Bell (Australia) and (n) St. Ives (Australia). The
963 REE content is normalized to Sun and McDonough (1989).

964 S10. Rare earth elements variations with zoning in tourmaline from orogenic gold deposits from LA-ICP-MS data; (a)
965 St. Ives (Australia); (b) Royal Hill (Rosebel, Suriname); (c) Young Davidson (Canada); (d) Hollinger (Canada); (e) Hoyle
966 Pond (Canada) and (f) Hira Buddini (India).

967 S11. Rare earth element patterns in tourmaline from (a) the Lincoln Hill gold deposit (USA), (c) hydrothermal veins
968 cutting the VMS mineralization at LaRonde (Canada) and (c) Roberto pegmatite (Canada).

969 S12. Variation of the REE patterns with the optical zoning in Roberto pegmatite.

970 S13. Trace element binary plots for tourmaline from various deposit types and rocks (a) Y vs Zr, (b) Ta vs Nb, (c) Th
971 vs U, (d) Ga vs Sn, (e) Sc vs V, (f) Ta vs Zr, (g) Li vs Be, (h) Sr/Sn vs Ba/Ga, and (i) Ta vs U. Data from the literature:
972 Jiang et al. (2002); Deksissa and Koeberl (2004); Roberts et al. (2006); Hazarika et al. (2015); Hazarika et al. (2016);
973 Grzela (2017); Kalliomäki et al. (2017) and Manégliá (2017).

974 S14. Trace element binary plots for tourmaline from various deposit types and rocks (a) V vs Sr, (b) Sn vs Zn/Nb, (c)
975 Sn vs Co/Nb, (d) V vs Ni, (e) Sn vs Sr/Ta, (f) Sn vs Co/La, (g) V vs Cr, (h) Sr/Sn vs Ni/Nb, and (i) Sr/Sn vs V/Be. Data
976 for orogenic gold deposits: Jiang et al. (2002); Deksissa and Koeberl (2004); Roberts et al. (2006); Hazarika et al.
977 (2015); Hazarika et al. (2016); Grzela (2017); Kalliomäki et al. (2017) and Manégliá (2017).

978

979

Table 1. Geological settings of studied gold deposits.

Deposits ¹	Metamorphic facies	Main country rock	Minor country rock	Mineralization age	References
Canadian shield					
Dome , Timmins, Canada	Greenschist	Tholeiitic basalt-komatiite	Mudstone-sandstone-conglomerate	<2679-2633±6 Ma	Proudlove et al. (1988); Moritz and Crocket (1990); Poulsen et al. (2000)
Hollinger , Timmins, Canada	Greenschist	Tholeiitic basalt	Unclassified granitoid, unclassified sediments	<2673 Ma	Smith et al. (1984); Wood et al. (1986); Smith et al. (1987); Schneider et al. (2012)
Hoyle Pond, Timmins, Canada	Greenschist	Tholeiitic basalt, basalt, komatiite		2660-2640 Ma	Dinel et al. (2008); Schneider et al. (2012)
Young Davidson, Matachewan, Canada	Greenschist	Syenite		2661 Ma	Martin (2012); Zhang et al. (2014b)
Canadian Malartic , Canada	Greenschist	Clastic sedimentary rocks	Subalkaline porphyritic quartz monzodiorite, granodiorite	2664 Ma	De Souza et al. (2014); De Souza (2015); El Goumi et al. (2015)
Roberto , Canada	Amphibolite	Turbiditic rocks		2675-2603 Ma	Ravenelle et al. (2010); Dubé et al. (2011); Ravenelle (2013); Fontaine et al. (2014); Fontaine et al. (2015)
James Bay, Canada	Greenschist			2.7-2.6 Ga	Hanes et al. (2017)
Wedding TR98-111		Basalt			
As		Intermediate to mafic volcanic			
Veine Marylou		Tonalite	Ultramafic dyke		
Orezone		Sedimentary rocks, felsic volcanoclastics			
		Gabbro			
North American Cordillera					
Excelsior, USA	Greenschist	Granite, granodiorite		162±5 Ma	https://mrdata.usgs.gov/mrds/s-how-mrds.php?dep_id=10310646 Taylor et al. (2015)
Amazonian craton					
Rosebel district, Suriname	Greenschist	Turbiditic and arenitic rocks	Basalt, andesite, rhyolite, felsic to intermediate tuff	2023-1955 Ma	Daoust et al. (2011)
Royal Hill Pay Caro					
Massif Central					
Salsigne , France	Greenschist	Siliciclastic and carbonate rocks		Late Carboniferous	Reynolds (1965); Marcoux and Lescuyer (1994); Demange et al. (2006)
West African craton					

Essakane, Burkina Faso	Lower greenschist	Turbiditic rocks		Proterozoic	IAMGold (2009)
Damara orogen Navachab, Namibia	Amphibolite	Sedimentary rocks including marble, calc-silicate rock and biotite schist		540-550 Ma	Nörtemann et al. (2000); Kisters (2005); Wulff (2008); Dziggel et al. (2009)
Kaapvaal craton New Consort, South Africa	Upper amphibolite	At the contact between mafic and ultramafic volcanic rocks and sedimentary rocks		3030 Ma	Otto (2007); Otto et al. (2007)
Dharwar craton Hira Buddini, India	Amphibolite	Basalt	Dacite, gabbro	2550-2530 Ma	Kolb et al. (2005); Krienitz et al. (2008); Hellmann (2009)
Uti, India	Amphibolite	Basalt		2550-2530 Ma	Kolb et al. (2005); Mishra et al. (2005)
Yilgarn craton Big Bell , Australia	Amphibolite	Basalt, komatiite		2662±5 Ma	Chown et al. (1982); Phillips and Nooy (1988); Wilkins (1993); Mueller et al. (1996)
St. Ives , Australia Britannia	Upper greenschist	Gabbro Basalt, komatiite	Sedimentary rocks	2650 Ma	Neumayr et al. (2008); Blewett et al. (2010); McGoldrick et al. (2013)

¹In **bold**: deposit with more than 70 t Au considered to be world-class after Goldfarb et al. (2005)

Table 1. Characteristics of tourmaline for each gold deposit.

Deposits	Thin Section	Mineral texture	Zoning	Core color ⁽¹⁾	Rim color ⁽¹⁾	Mineral associations
Dome, Canada	4	Very fine grained aggregates	Subtle	Orange	Orange	qz, ms, bt, carb, py, cpy, rt
Hollinger, Canada	2	Fine grained aggregate anhedral	Subtle to weak	Brown	Colorless to brown	qz, carb, ser, py, cpy, rt
Hoyle Pond, Canada	11	Fine to coarse grained aggregate	Weak	Bluish grey or orange	Orange	qz, carb, ser, bt, py, cpy, apy, gold
Young Davidson, Canada	1	Isolated coarse grain	Weak	Beige to dark greenish brown	Lighter than the core color	ksp, mc, qz, carb, rt, hem, gold
Canadian Malartic, Canada	3	Medium grained aggregate	Moderate	Bluish grey	Brownish green Locally orange	qz, mc, or, carb, py, cpy, sp, rt, mag
Roberto, Canada	9	Disseminated fine grained sub-rounded	Subtle Subtle to weak	Orange Light to dark greenish brown	Orange Light to dark greenish brown	qz, mc, apy, po
James Bay, Canada Wedding	2	Massive aggregate of medium grained anhedral to subhedral for all showings	Subtle to weak	Light to dark brown	Light to dark brown	qz, carb, py, cpy, rt
TR98-111	1		Subtle to strong oscillatory	Bluish green	Bluish green	qz, py, rt
As	2		Subtle to weak	Bluish grey	Light brown	qz, py, ser, rt
Veine	3		Subtle to weak	Bluish grey to light brown	Green	qz, cpy
Marylou	4		Subtle to moderate	Bluish grey to orange brown	Orange brown	qz, apy, py
Orezone	1		Subtle	Bluish grey	Brownish green	qz, bt, carb, rt
Excelsior, USA	1	Disseminated medium grain acicular in fan shape	Subtle to irregular	Dark green to light brown	Dark green to light brown	qz, bt, ser, py, mag, po, cpy
Rosebel district, Suriname Royal Hill	9 3	Aggregate to disseminated of medium grain subhedral to euhedral	Subtle to strong	Brown to bluish green	Bluish green	qz, carb, ser, chl, py, apy, rt, gold
Pay Caro		Fine grained disseminated acicular	Subtle	Greenish blue	Greenish blue	qz, carb, ser, chl, py, rt, mag
Salsigne, France	3	Fine grained disseminated to small aggregate of subhedral grains	Subtle	Orange to light blue	Orange	qz, ser, bt, chl, apy, py, sp

Essakane, Burkina Faso	21	Fine to very fine grained acicular disseminated to massive aggregate	Subtle to weak	Orange	Light orange	qz, carb, pl, ser, sch, py, apy, rt, Gold
Navachab, Namibia	1	Fine grained disseminated	Subtle to weak	Greenish brown	Greenish brown	qz, carb, py, cpy
New Consort, South Africa	4	Fine to medium grained disseminated to massive aggregates	Weak irregular	Dark brown to light grey	Light to dark brown	qz, pl, ser, bt, hbl, py, po, apy, cpy, rt, hem, po
Hira Buddini, India	3	Medium grained disseminated subhedral to massive aggregate of very fine anhedral grains	Weak irregular	Dark brownish green	Brownish green	qz, ksp, pl, ser, amp, bt, py, rt
Uti, India	1	Disseminated fine grained euhedral	Absent	Brownish orange	Brownish orange	qz, ms, carb, rt
Big Bell, Australia	1 ⁽²⁾	Fine grained or 1-2 mm porphyroblasts				Lo, apy, mag
St-Ives, Australia Britannia	2	Medium to coarse grained subhedral disseminated	Irregular	Greenish blue	Green	qz, carb, ms, py, rt, gold

⁽¹⁾ The core and the rim color refers to the color under optical microscope

⁽²⁾ grains mounted in polished section

Mineral abbreviations: ab: albite, ap: apatite, apy: arsenopyrite, cal: calcite, carb: carbonate, chl: chlorite, cpx: clinopyroxene, cpy: chalcopyrite, grt: garnet, hem: hematite, mag: magnetite, mc: microcline, ms: muscovite, pl: plagioclase, po: pyrrhotite, py: pyrite, qz: quartz, rt: rutile, ser: sericite, sulf: sulfide, tur: tourmaline.

NA: Not Available

Table 1. Median trace element compositions in tourmaline from orogenic gold deposits divided by the metamorphic facies of the country rocks.

(ppm)	Lower greenschist to lower amphibolite (with the exception of Canadian Malartic)	Middle to upper amphibolite
Ga	32.5	64.6
Sn	1.0	10.5
Σ REE	0.94	12.75
Σ LREE	0.55	11.05
Σ HREE	0.11	0.18
Hf	0.019	0.084
Nb	0.014	0.129
Ta	0.006	0.043
Y	0.122	0.300
U	0.006	0.057
Th	0.010	0.017
Ti	2036	5585

Figure 1

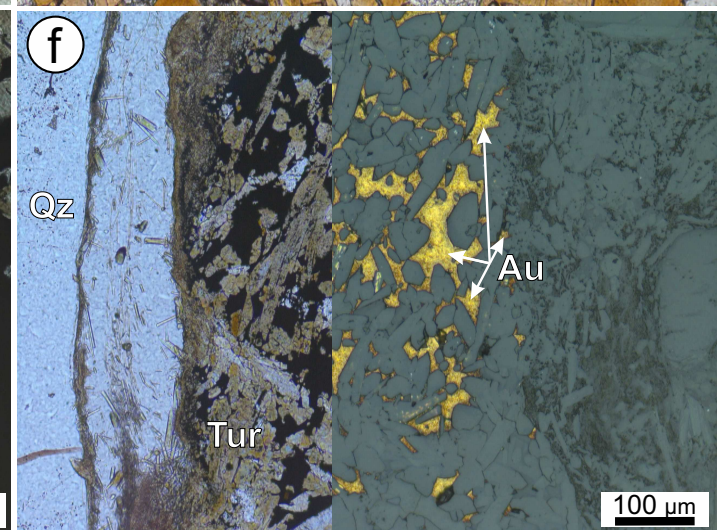
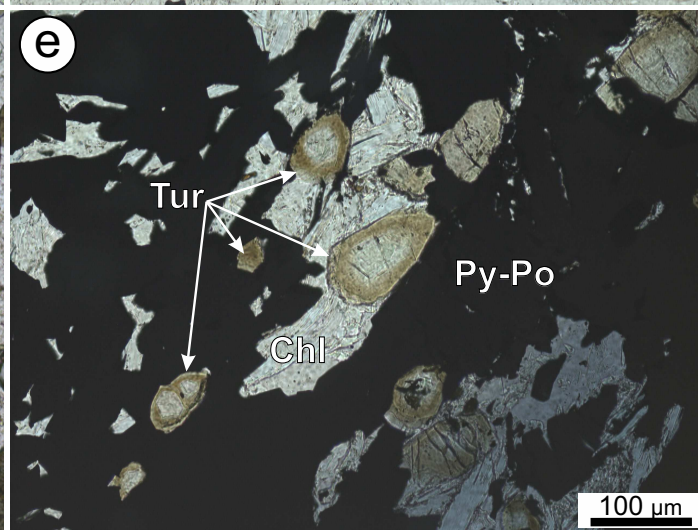
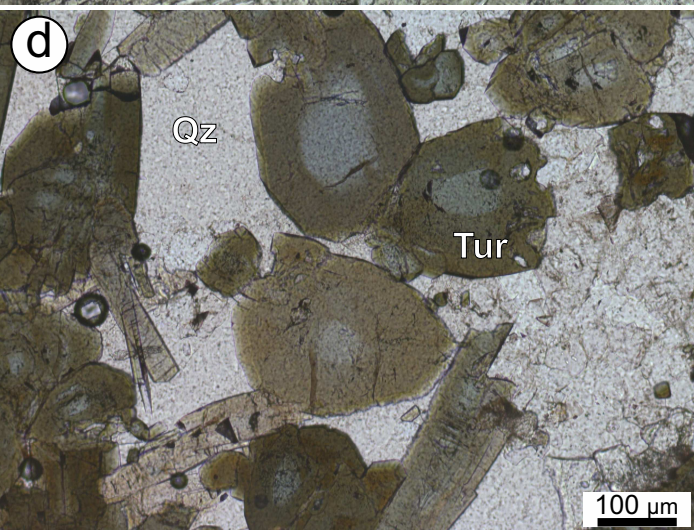
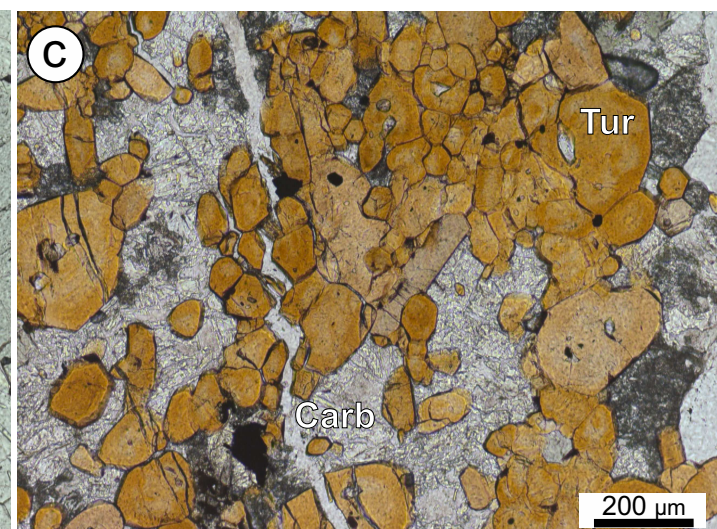
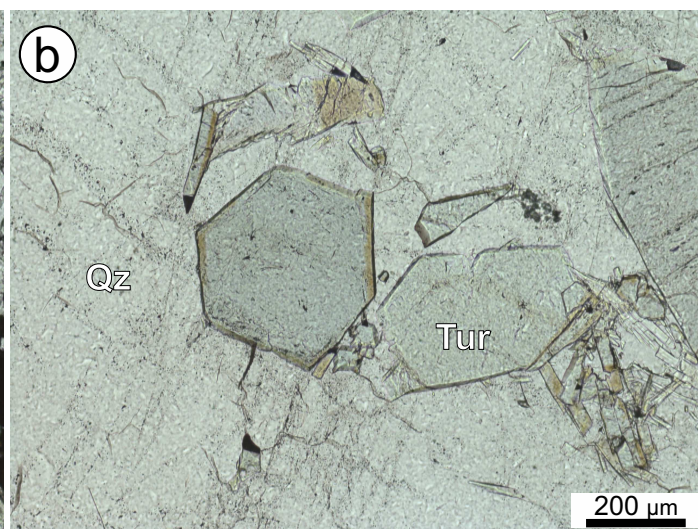
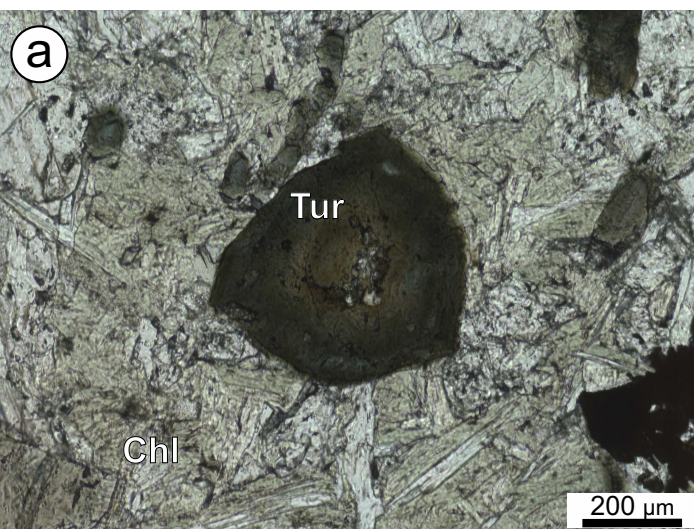


Figure 2

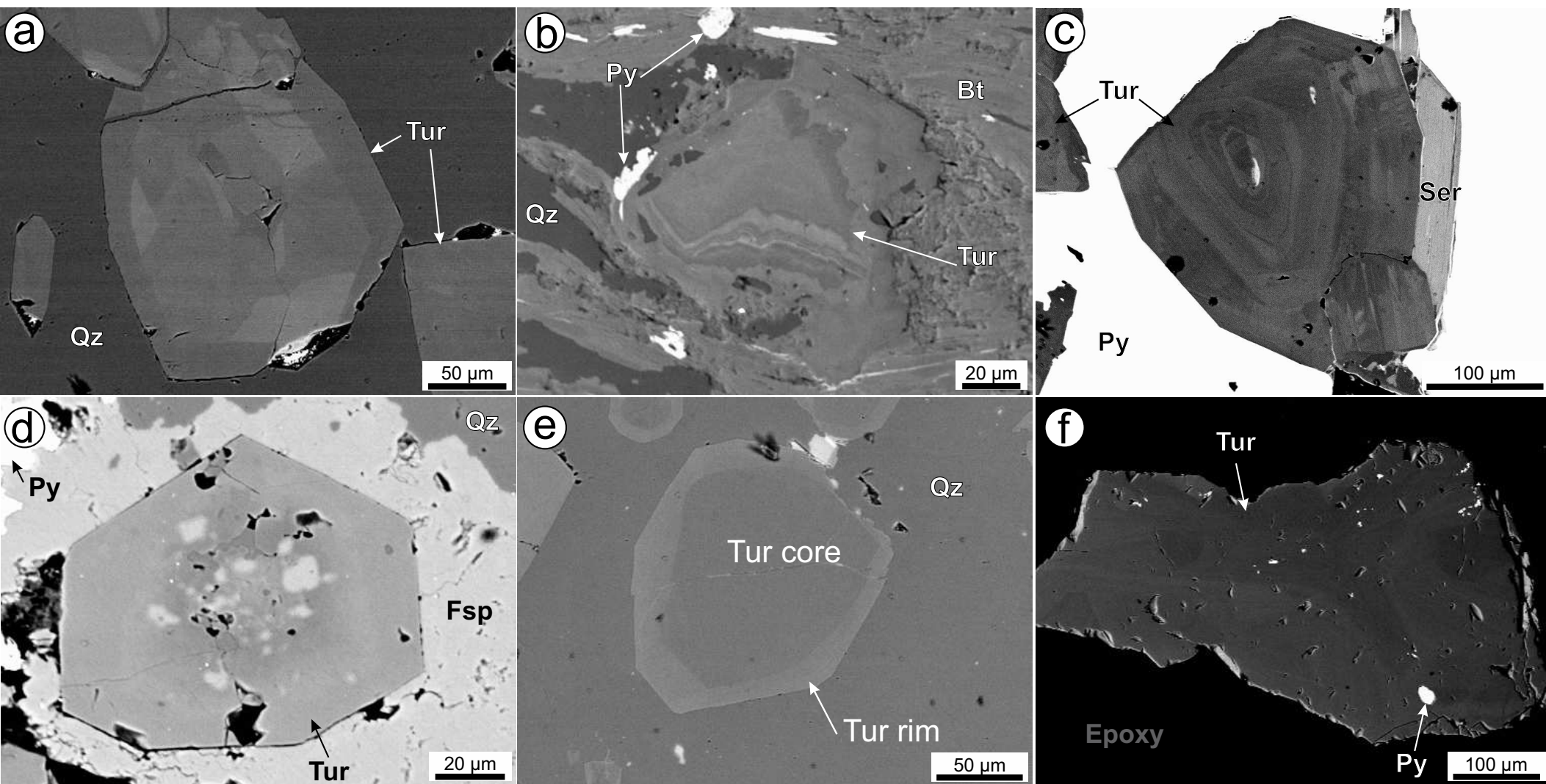


Figure 3

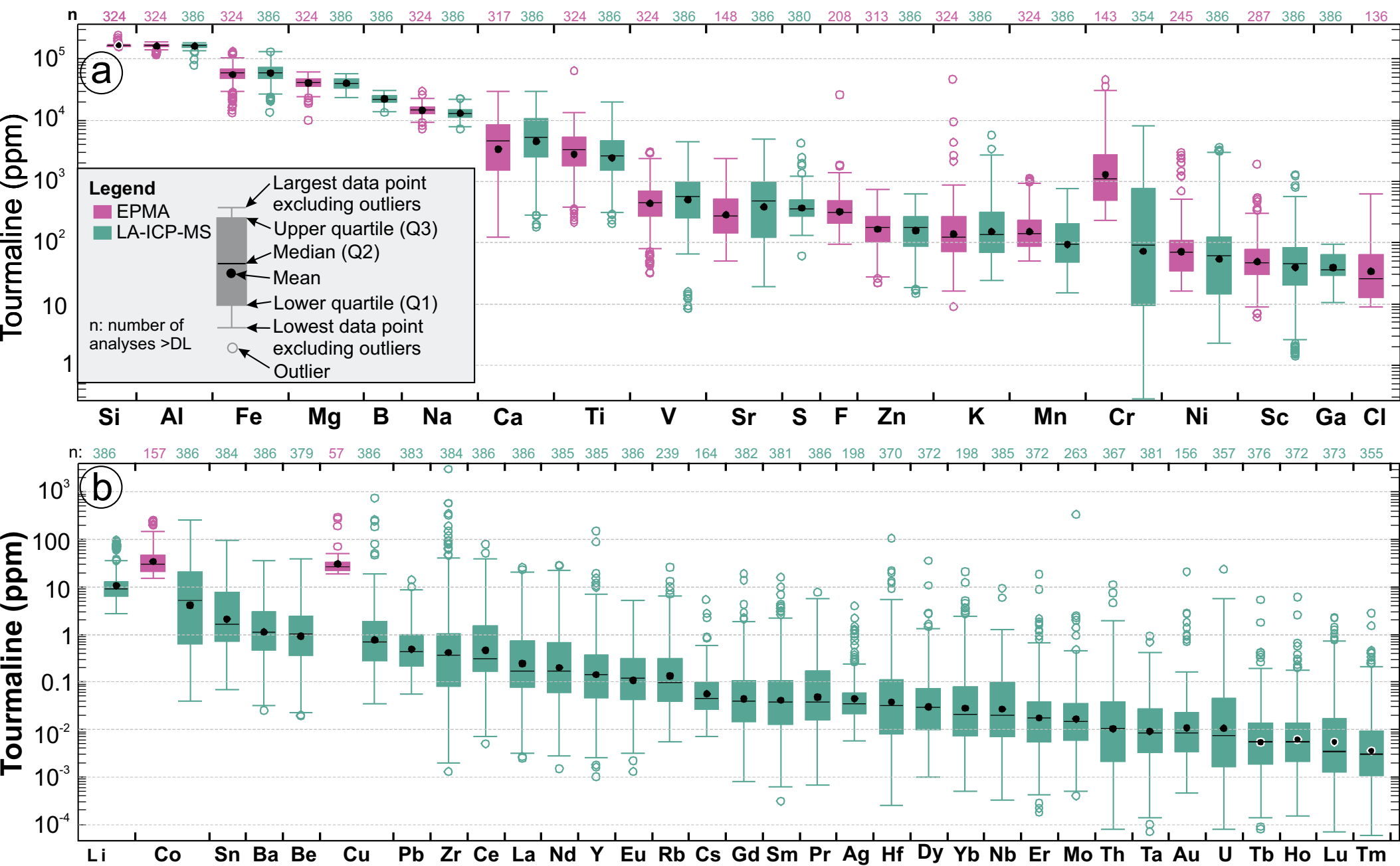


Figure 4

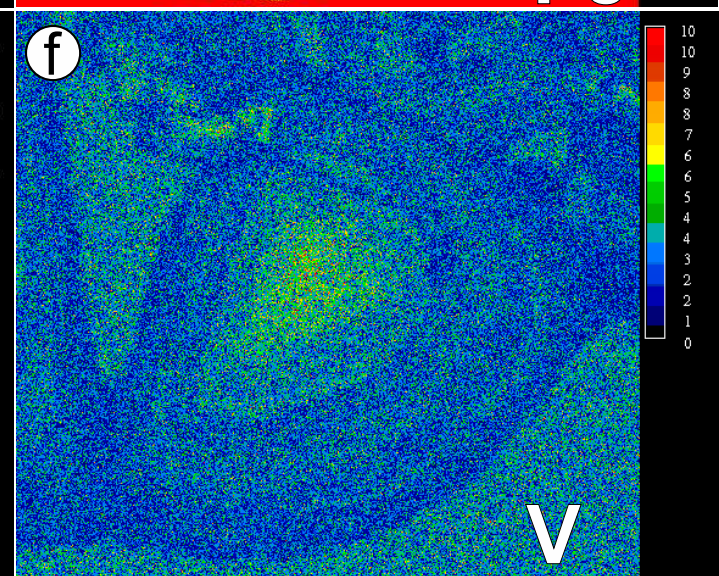
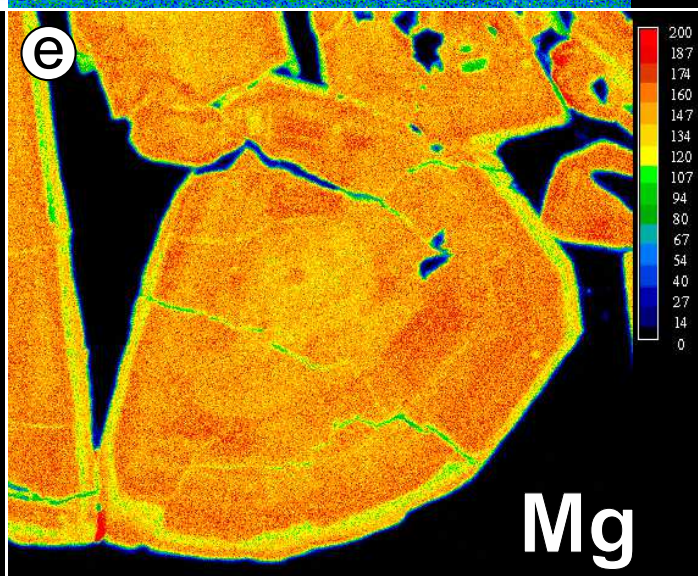
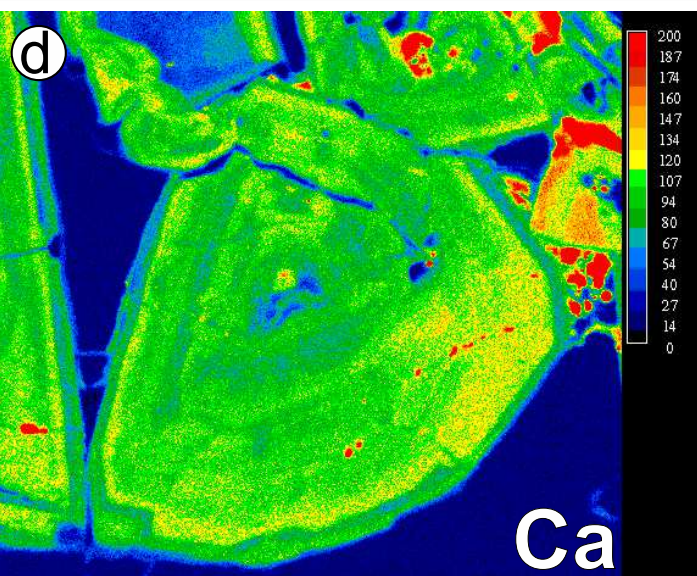
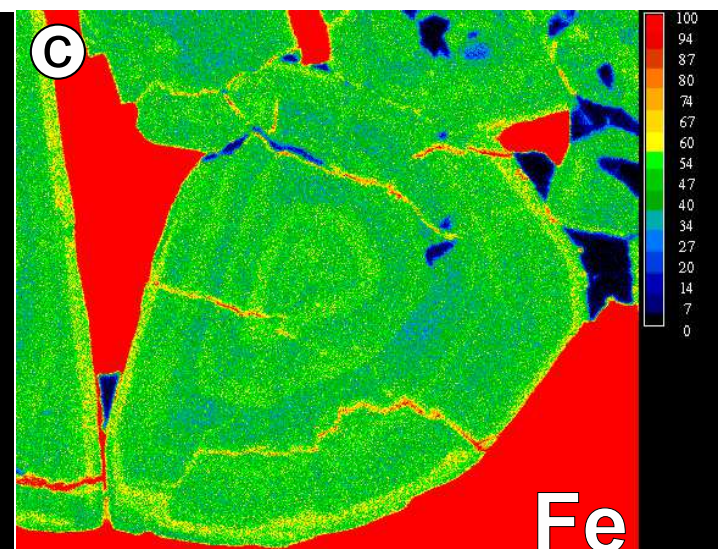
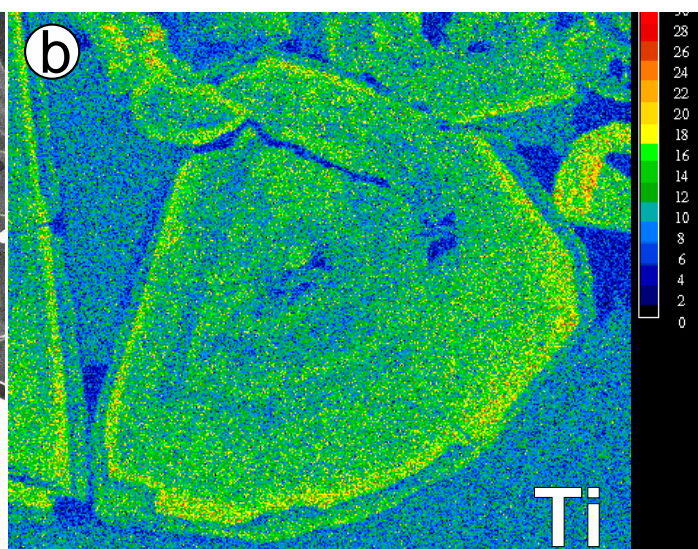
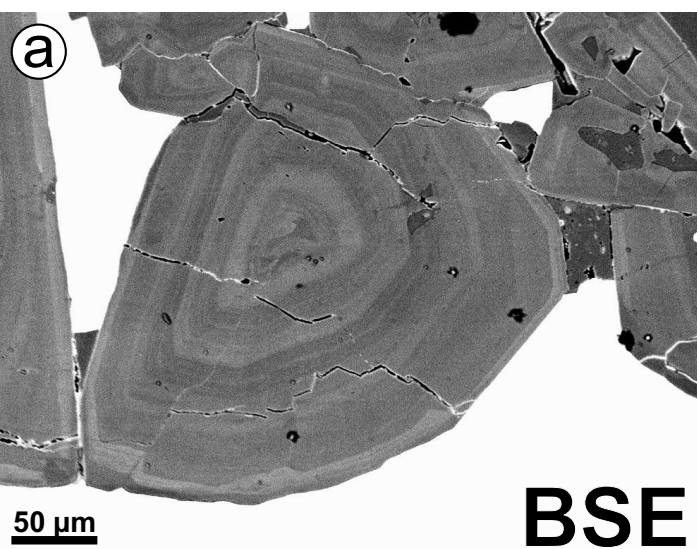
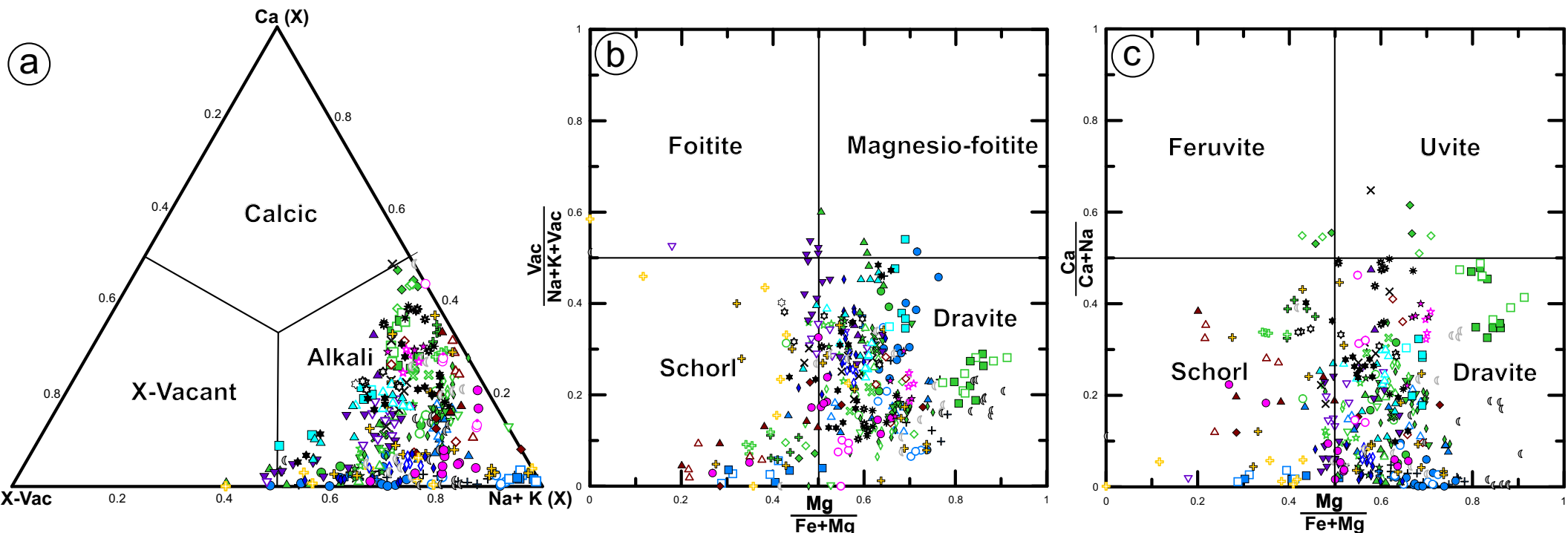


Figure 5



Zone									
◇ Rim	◇ Core/unzoned grain								
Orogenic gold deposits									
⊕ Hollinger	● Hoyle Pond	Roberto	James Bay	▲ Excelsior	Rosebel	⊕ Salsigne	✕ Navachab	● Hira Buddini	□ Big Bell
⊕ Dome	□ Young Davidson	■ Orange tourmaline	● Veine	▼ TR98-111	▼ Royal Hill	◆ Essakane	☾ New Consort	★ Uti	▲ St-Ives
	▲ Canadian Malartic	◇ Brown tourmaline	▲ As	◇ Marylou	▲ Pay Caro				
			★ Wedding	✕ Orezone					
Other gold deposit	Pegmatite	Metamorphic tourmaline	Hydrothermal vein						
◆ Lincoln Hill	⊕ Roberto pegmatite	* Tehery Wager	* LaRonde						

Figure 6

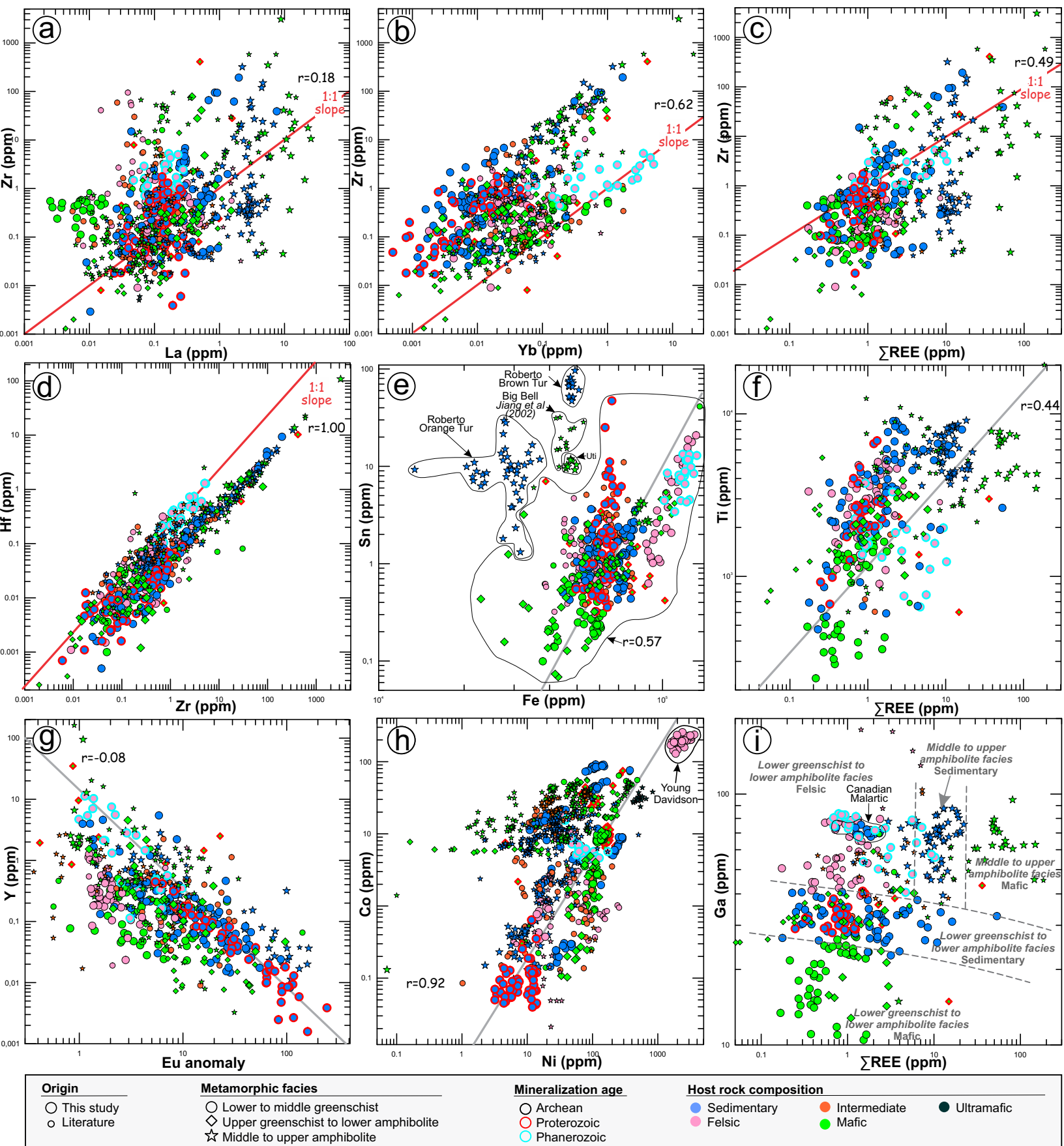


Figure 7

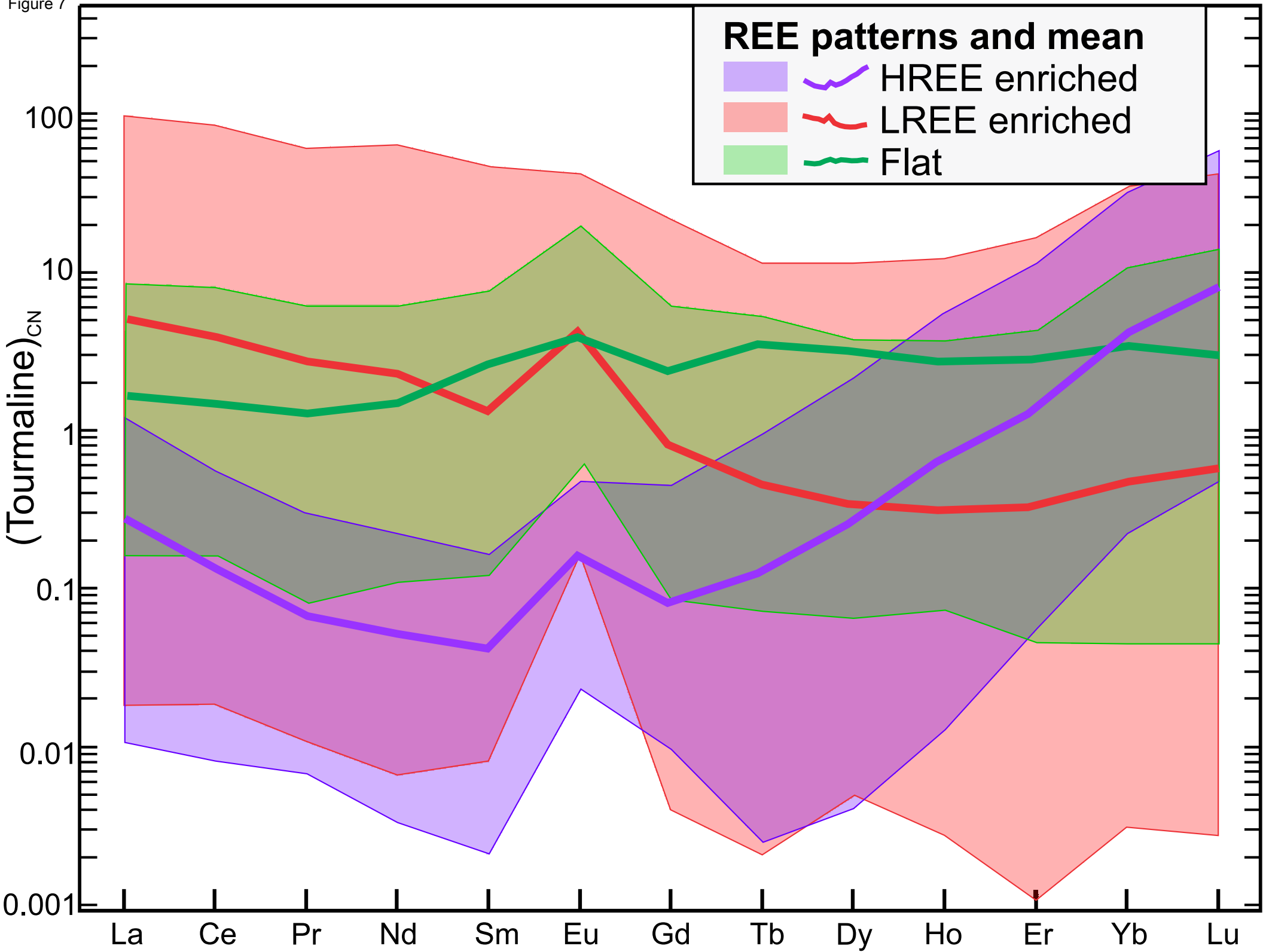
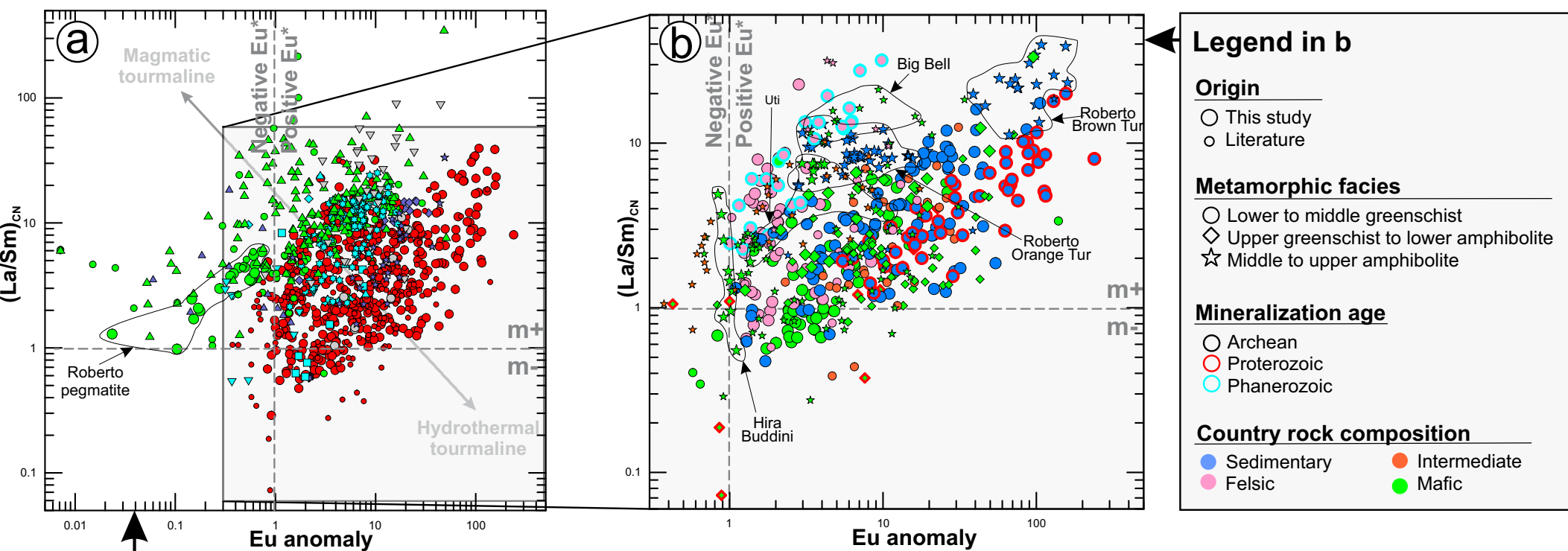


Figure 8



Legend in a

Metamorphic

- **Orogenic gold** (this study)
- **Orogenic gold** (Grzela 2017, Kalliomäki et al. 2017, Manéglia 2017, Hazarika et al. 2016, Hazarika et al. 2015, Roberts et al. 2006, Jiang et al. 2002)
- **Metamorphic** (Berryman et al. 2017)
- ▽ **Amphibolite** (Wang et al. 2018)

Hydrothermal

- ◆ **Lincoln Hill gold deposit** (this study)
- ▲ **Sn-Pb-Zn stratiform** (Jiang et al. 1999)
- ★ **U-unconformity related** (Joyce et al. 2016)
- ★ **Hydrothermal veins at LaRonde** (this study)

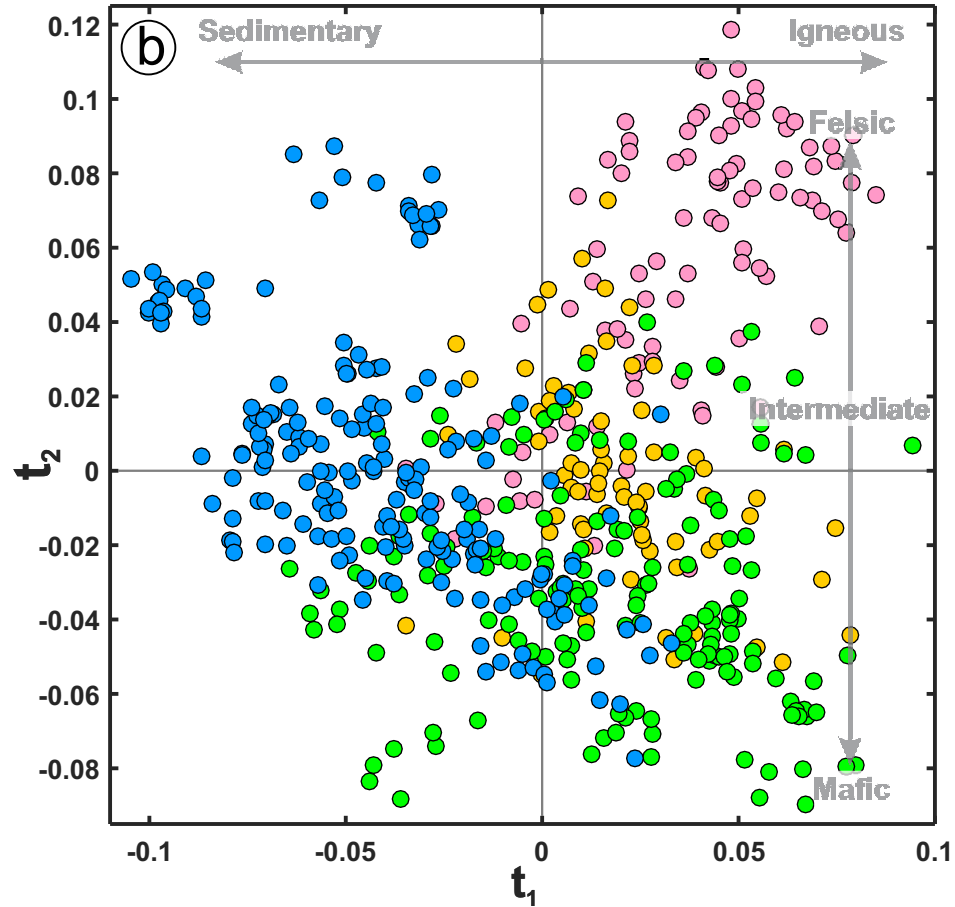
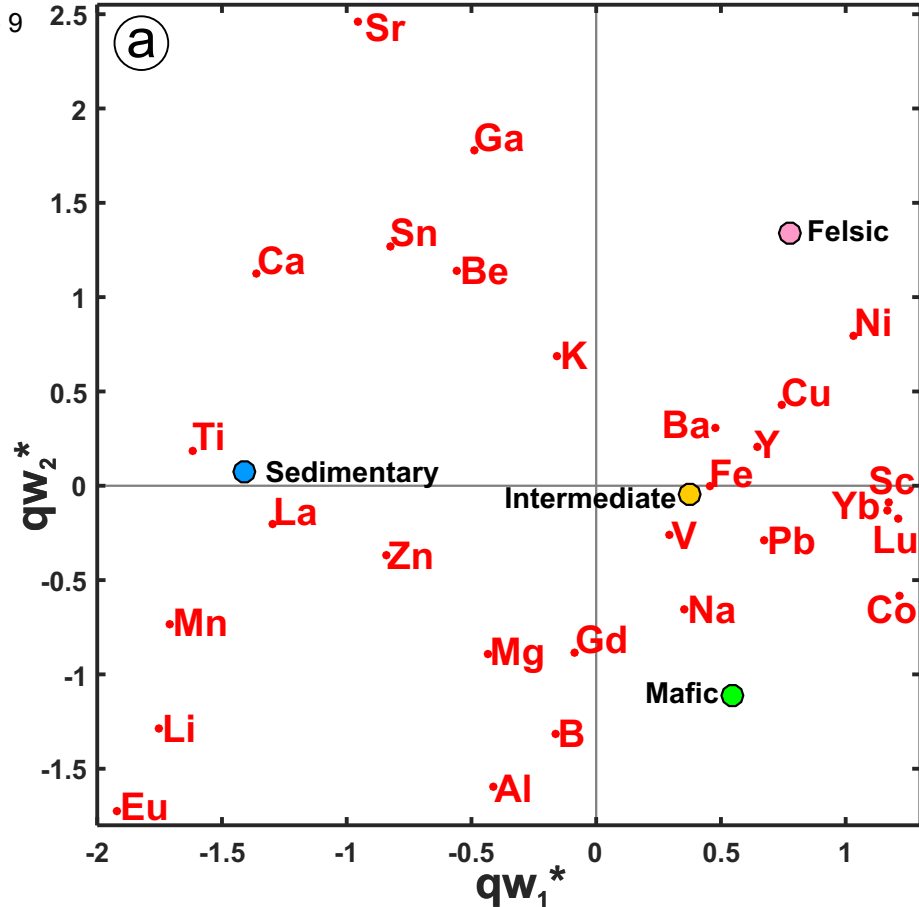
Magmatic-hydrothermal

- ◆ **Porphyry Cu-Mo** (Iveson et al. 2016)
- **W(-Sn) mineralization** (Harlaux 2016)
- ▽ **Sn skarn** (Jiang et al. 2004)
- ★ **Sn deposit** (Harlaux et al. 2018)
- ▲ **Magmatic hydrothermal** (Hong et al. 2017)

Magmatic

- **Pegmatite** (this study, Hazarika et al. 2017, Iveson et al. 2016, Roda-Robles et al. 2015, Čopjaková et al. 2013, Bačík et al. 2012, Gadas 2012, Roda-Robles et al. 2011, Raith et al. 2004, Jolliff et al. 1987, Laul and Lepel 1987)
- ▲ **Granite** (Harlaux et al. 2018, Hong et al. 2017, Kalliomäki et al. 2017, Tahmasbi et al. 2016, Čopjaková et al. 2015, Yang et al. 2015, Pesquera et al. 2005, Raith et al. 2004, Ward et al. 2012)

Figure 9



Country rock composition

● Felsic
 ● Intermediate
 ● Mafic
 ● Sedimentary

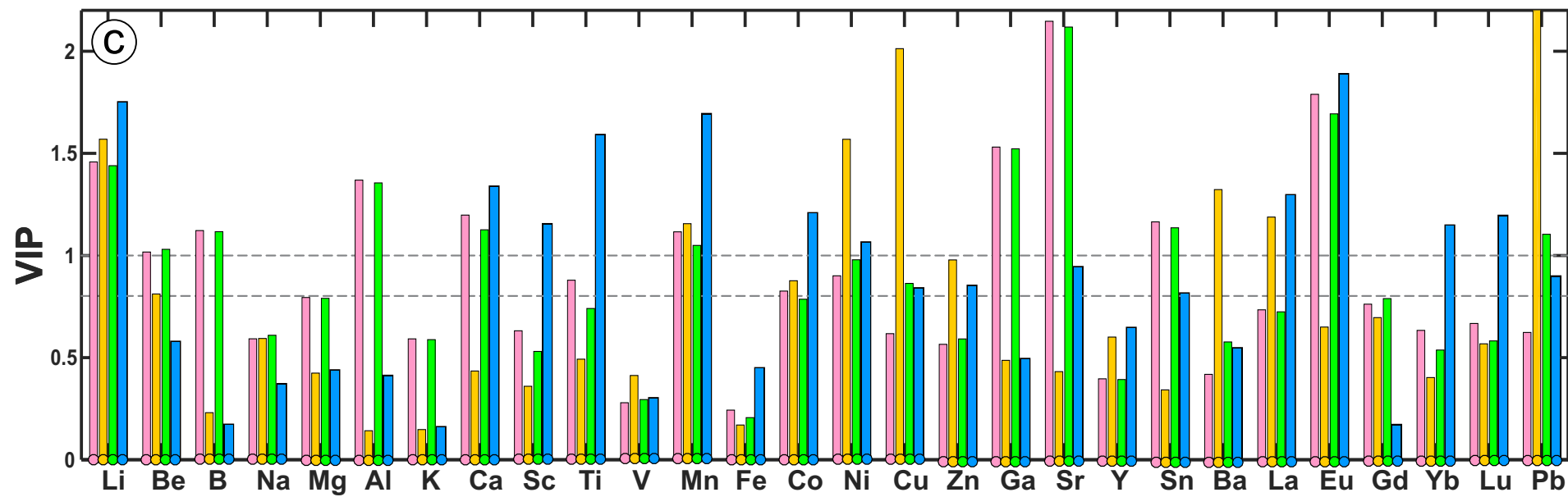
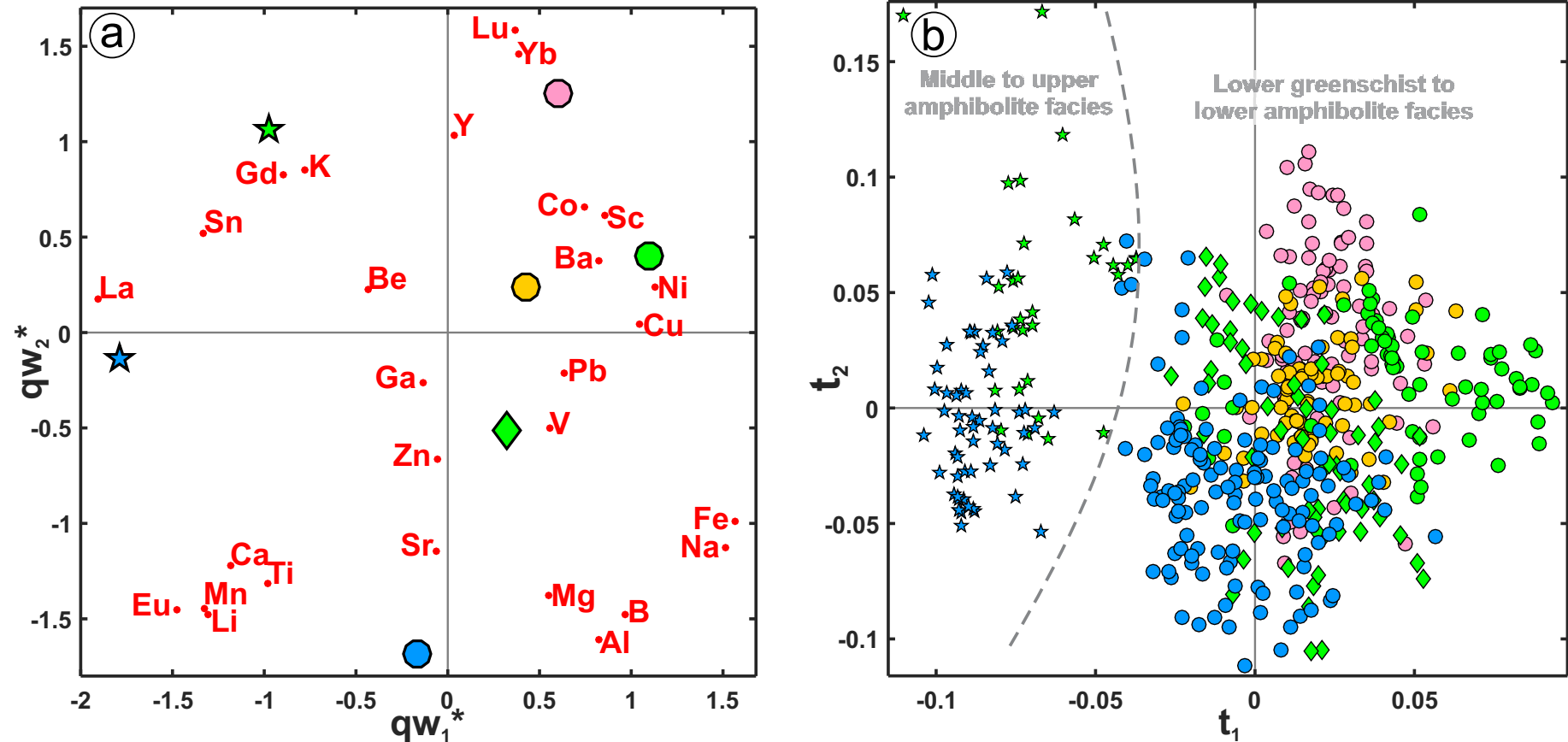


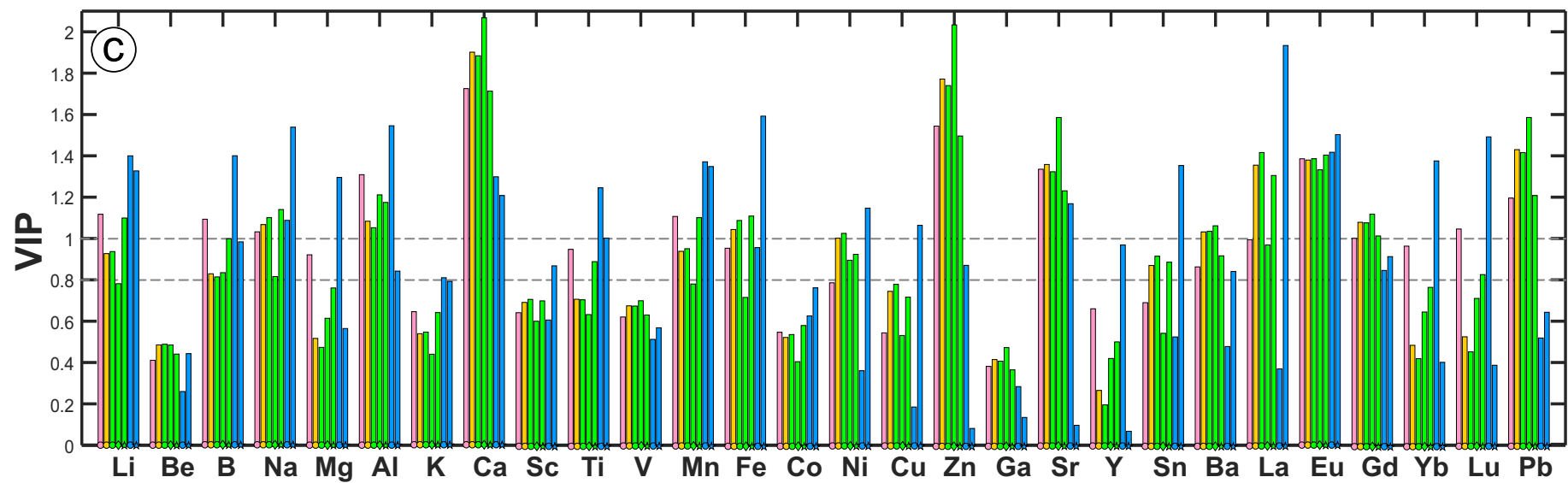
Figure 10

**Country rock composition**

● Felsic
 ● Intermediate
 ● Mafic
 ● Sedimentary

Metamorphic facies of the country rock

○ Lower to middle greenschist
 ◇ Upper greenschist to lower amphibolite
 ★ Middle to upper amphibolite



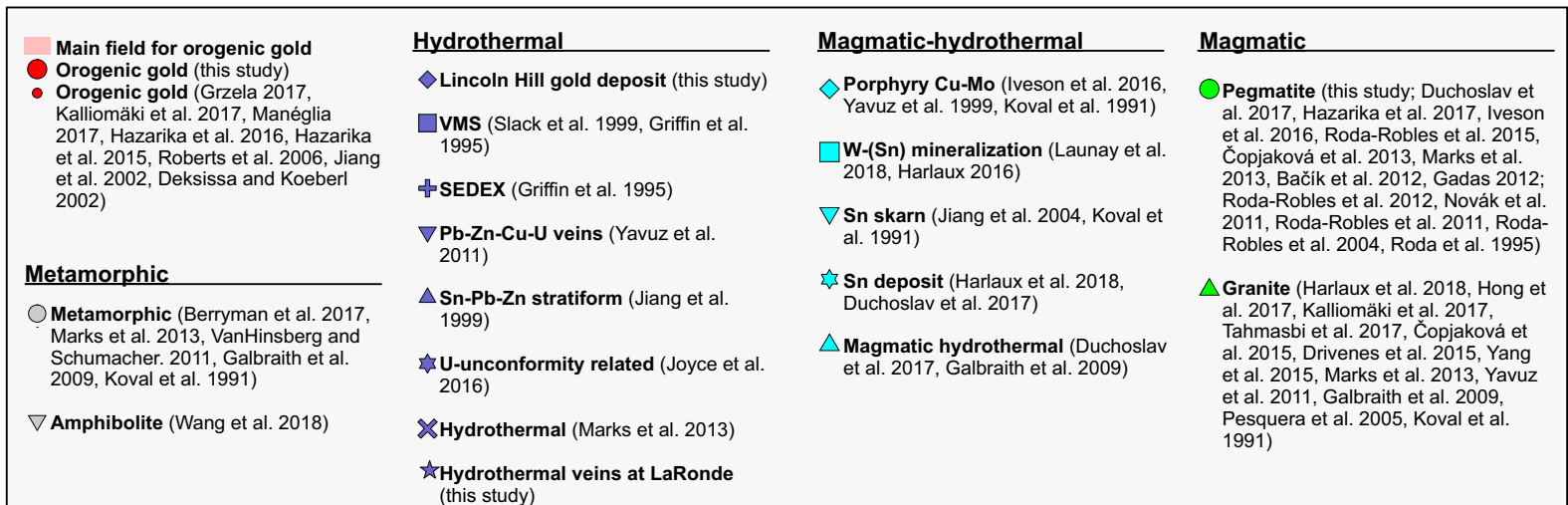
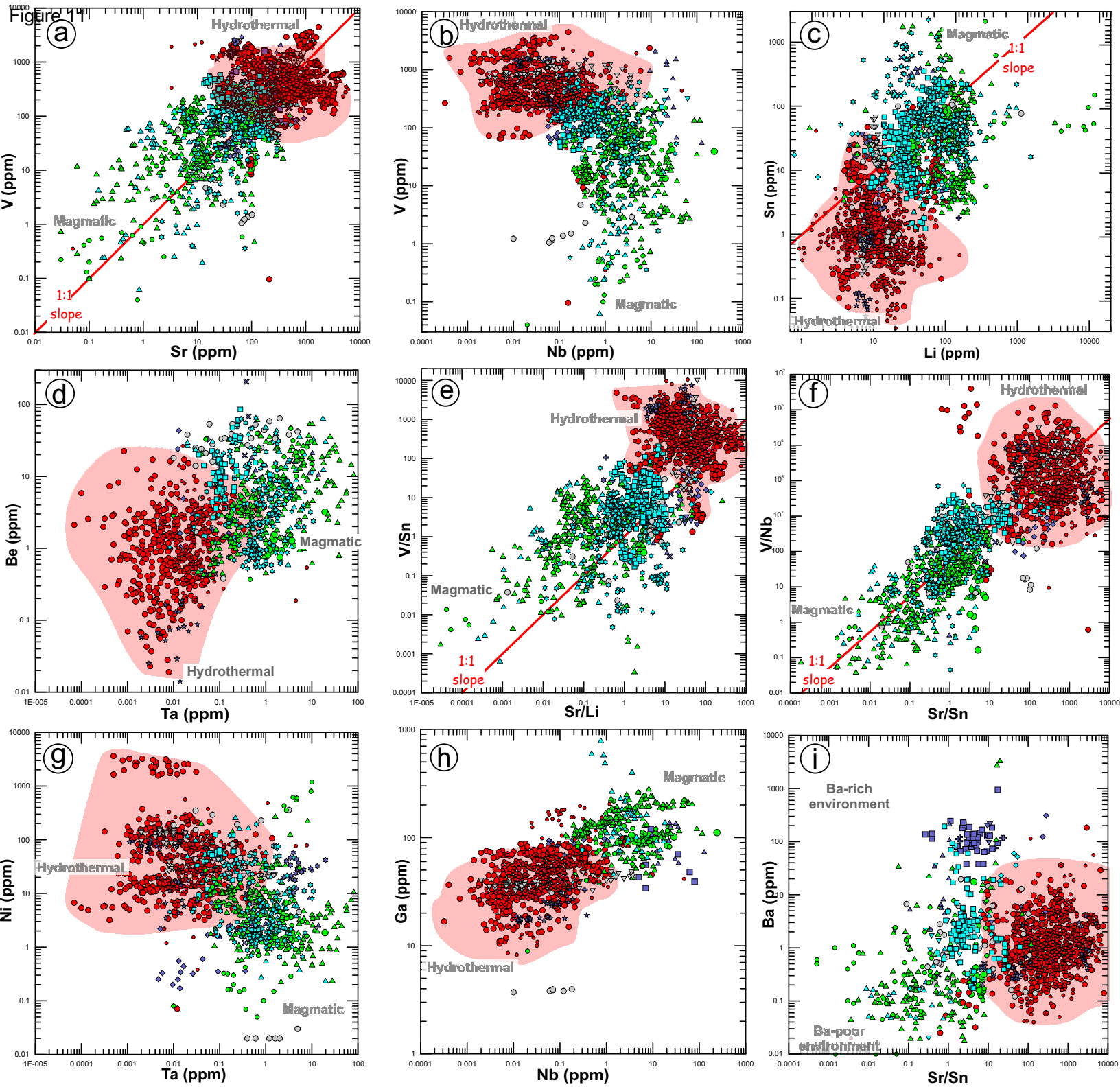
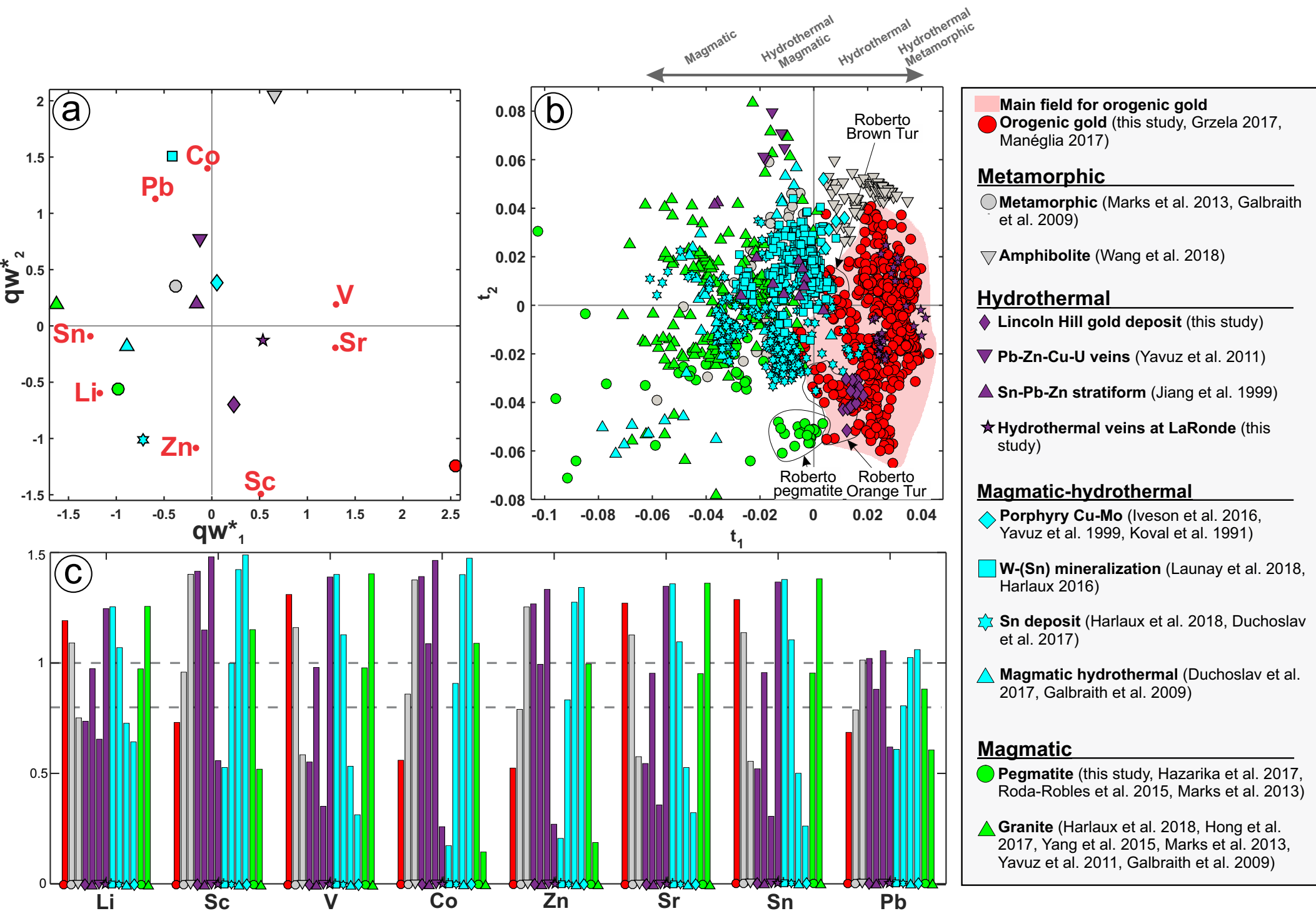
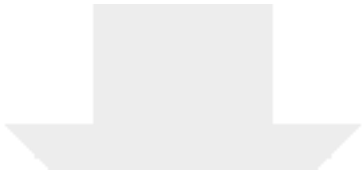



Figure 12





Click here to access/download
Supplementary Material
ESM01.xlsx





Click here to access/download
Supplementary Material
ESM02_20200325.pdf

